Itaconate transport across the plasma membrane and *Salmonella*-containing vacuole via MCT1/4 modulates macrophage antibacterial activity

Qingcai Meng[1, 3], Chengxi Li[1, 3], Yuping Cai[2], Ying Chen[1], Xiaoqing Chen[1], Xin Wang[1], Biling Zhang[1], Yue Zhang[1], Feng Liu[1], Meixin Chen[1]*

[1] Institute of Infectious Diseases, Shenzhen Bay Laboratory, Shenzhen, 518132, China.

[2] Interdisciplinary Research Center on Biology and Chemistry, Shanghai Institute of Organic Chemistry, Chinese Academy of Sciences, Shanghai, China.

[3] These authors contributed equally to this work.

*Correspondence: chenmx@szbl.ac.cn

Abstract

Itaconate accumulates and manifests antibacterial activity in macrophages upon bacterial infection. Convincing evidence substantiates that itaconate transports across the plasma membrane and vacuolar membrane. But the molecular bases underlying the bidirectional transport of itaconate across membranes and how it affects intracellular bacterial replication remain elusive. Here, we identify MCT1 and MCT4 as bidirectional transporters of itaconate. In addition to modulating itaconate concentration as transporters at the plasma membrane, MCT1 and MCT4 function as itaconate transporters at *Salmonella*-containing vacuole (SCV). Upon *Salmonella* infection, MCT1 and MCT4 transport itaconate into SCV facilitated by RAB32. Itaconate is also secreted out of cells through MCT1 and MCT4 as the infection persists. The suppression of MCT1 and MCT4-dependent itaconate secretion generally increases the concentration of itaconate and the prevalence of itaconate-targeted *Salmonella* intracellularly, consequently inhibiting *Salmonella* replication. Our study offers valuable insights into itaconate transport during bacterial infection and sheds light on the development of itaconate-dependent therapeutic strategies.

Introduction

The bacterial infection leads to a dramatic metabolic shift in cells of hematopoietic origin, which is a crucial event of cell-autonomous defenses[1-3]. The activation of macrophages by bacteria undergoes enhanced glycolysis and disturbed tricarboxylic acid (TCA) cycle. The break at isocitrate dehydrogenase 1 (IDH1) of the TCA cycle results in increasing cis-aconitate[4]. Subsequently, the highly expressed immune-responsive gene 1 (IRG1, also known as aconitate decarboxylase 1, ACOD1) catalyzes the decarboxylation of cis-aconitate into itaconate[2,5]. Itaconate has been reported to regulate immune responses by modifying proteins known as "itaconation"[6] as well as "itaconylation"[7,8]. Alternatively, itaconate works as a well-established antibacterial metabolite[9-12], coordinated decently by the RAB32-LRRK2 complex as illuminated in our previous study[13,14]. In the context of antibacterial immunity and immunoregulation, maintaining optimal intracellular itaconate concentration is crucial[15,16]. And the potential transport of itaconate through plasma membrane or itaconate delivery into bacteria-containing vacuole has been mentioned in various scenarios[13,17-20]. The bidirectional transporters for itaconate likely exist, given its limited cell permeability[16,21]. More recently, ABCG2 has been recognized as an exporter of itaconate at plasma membrane[22]. But the absence of ABCG2 did not completely block the secretion of itaconate from macrophages[22], which prompts us to study more about itaconate transport. Overall, currently, the bidirectional transporter(s) at the plasma membrane or bacteria-containing vacuole remains unknown[21].

Solute carrier (SLC) proteins belong to a major transporter superfamily[23], which has been demonstrated as metabolic gatekeepers at the plasma membrane or vacuoles in various cell types, including macrophages[24,25]. For instance, MCT1 (SLC16A1) facilitates succinate release from muscle tissue[26]. SLC13A5 is a well-established citrate transporter[27]. SLC7A11 primarily functions as a cystine/glutamate exchanger, focusing on transporting cystine and glutamate[28]. SLC1A5 primarily transports neutral amino acids, especially glutamine[29]. SLC39A7 facilitates the uptake of zinc ions into cells, playing a critical role in zinc homeostasis. SLC22A1, also known as OCT1 (Organic Cation Transporter 1), is involved in the transport of organic cations[30]. However, little is known about the role of SLC proteins in transporting antibacterial metabolites during bacterial

infection. In this study, we have identified MCT1 (SLC16A1) and MCT4 (SLC16A3) as itaconate bidirectional transporters at cell plasma membrane or bacteria-containing vacuole (BCV). Our findings connect the metabolic transporters MCT1/4 and anti-bacterial defense by dissecting their important roles in transporting itaconate.

Results

The inhibition of MCT1 and MCT4 transport activity resists *Salmonella* infection

We first verified itaconate secretion in bacteria-infected macrophages. Itaconate accumulated in the cytosol (~0.2-3 nmol/10^6 RAW264.7 cells) and subsequently released into the cell supernatant (~2-30 nmol/10^6 RAW264.7 cells) over time following infection with the gram-negative bacteria *Salmonella* **(Fig. 1a, b)**. A larger proportion of itaconate was secreted into the extracellular space during infection **(Fig. 1c)**, analogous to that observed in LPS-treated macrophages[20,31]. Based on this point, we reasoned that if itaconate transport across the plasma membrane has been dampened, the concentration of intracellular itaconate would be altered pronouncedly. As a result, it may influence the bacteria-eliminating effects of itaconate. Thus, to search for itaconate transporter(s), we first determined whether some available inhibitors of SLC transporters modulated the bacterial survival in cells. The concentrations of SLC inhibitors (for MCT1, MCT4, SLC13A5, SLC7A11, etc.) were established based on documented methodologies[28,29,32-40]. The survival of *Salmonella enterica serovar* Typhi (*Salmonella* Typhi) was remarkably inhibited in the presence of Su3118 (Syrosingopine, a dual inhibitor for MCT1 and MCT4)[41] in RAW264.7 cells **(Fig. 1d, e)** and bone marrow-derived dendritic cells **(Supplementary Fig. 1a)**. We further found that Su3118 attenuated the replication of the broad-host-range serotype *Salmonella enterica serovar* Typhimurium (*Salmonella* Typhimurium) **(Fig. 1f)**. VB124[42] (a MCT4 inhibitor) in combination with AZD3965[43] (a MCT1 inhibitor) also had a strong inhibitory effect on *Salmonella* proliferation in RAW264.7 cells **(Fig. 1g)**. Importantly, a lower bacterial load was detected in human monocyte-derived macrophages (hMDM) with MCT1 and MCT4 impairments **(Fig. 1h).** And these inhibitors themselves had no significant influence on *Salmonella* growth in a mammalian-cell-free system **(Supplementary Fig. 1b-d)**. We also examined whether

91 MCT1 or MCT4 (MCT1/4) inhibitors inhibited the phagocytic capacity of cells, which

92 probably led to the detection of a lower bacterial load in cells. We found that long-term

93 inhibition of MCT1 and MCT4 transport activity did not alter the entry of *Salmonella* into

94 bone marrow-derived macrophages (BMDMs), RAW264.7 cells or DC2.4 cells

95 **(Supplementary Fig. 1e-h)**. It indicates that blocking MCT1/4 does not affect

96 macrophage phagocytosis. We then constructed MCT1/4 depletion cell line by

97 CRISPR/Cas9 **(Supplementary Fig. 1i)**. It is worth noting that *Mct4$^{-/-}$* RAW264.7 cells

98 treated with the MCT1 inhibitor (AZD3965) sustained less bacterial replication **(Fig. 1i)**.

99 And the MCT4 inhibitor VB124 dramatically reduced bacterial load in *Mct1$^{-/-}$* RAW264.7

100 cells **(Fig. 1j)**. These data highlighted that the combinational defect in MCT1 and MCT4

101 enhances the antibacterial activity in macrophages.

102

103 However, the bactericidal effect of Su3118/(AZD3965+VB124) disappeared or reduced

104 in *Irg1*-deficient RAW264.7 cells or HeLa cells, which lacks endogenous itaconate

105 generation **(Fig. 1k, l and Supplementary Fig. 1j, k**). IRG1 expression in HeLa cells

106 rescued the bacterial-killing properties of Su3118/(AZD3965+VB124) **(Fig. 1m)**.

107 Consistently, the ablation of *Irg1* in mice led to the inefficiency of Su3118 in reducing

108 *Salmonella* load (**Fig. 1n**). Besides, we observed that the protein level of IRG1 and MCT4

109 concurrently increased in RAW264.7 cells, spleen, and liver after bacterial infection with

110 a modest change in mRNA level of MCT1/4 (**Fig. 1o, p and Supplementary Fig. 1l-o**).

111 Taken together, these data underlined the critical roles of MCT1 and MCT4 transport

112 activity in itaconate-dependent immune responses against bacterial infection, which

113 predicted that the solute carriers MCT1 and MCT4 were itaconate transporters.

114

The inhibition of MCT1 and MCT4 transport activity promotes the prevalence of

itaconate-targeted *Salmonella*

117 We next continued to explore the roles of MCT1 and MCT4 in regulating itaconate-based

118 bacterial killing. Markedly, MCT1 and MCT4 were detected to be located at the plasma

119 membrane in macrophages **(Fig. 2a and Supplementary Fig. 2a, b)**. The transport

120 activity of MCT1 and MCT4 at the plasma membrane may modify the level of itaconate

121   within cells. To better understand whether the MCT1 and MCT4-related restriction of

122   bacteria growth is metabolites-related, we profiled the metabolic changes of BMDMs

123   under various conditions. We have observed an accumulation of itaconate in BMDMs with

124   disrupted MCT1 and MCT4 transport activity through untargeted metabolomics **(Fig. 2b)**.

125   Spontaneously, succinate, lactate and pyruvate, which are also substrates of MCT1 or

126   MCT4, accumulated **(Fig. 2b)**. The inhibition of MCT1 and MCT4 also increased the

127   concentration of itaconate in RAW264.7 cells at the late stage of infection **(Fig. 2c).** We

128   also scrutinized whether a higher concentration of itaconate resulted in a greater number

129   of itaconate-targeting *Salmonella* Typhi. To do that, we took advantage of the

130   nanoluciferase-biosensor of itaconate located in bacteria as described before

131   **(Supplementary Fig. 2c)**[13]. We found that more bacteria were targeted by itaconate in

132   RAW264.7 cells when MCT1 and MCT4 activity was suppressed at the later phase of

133   infection **(Fig. 2d and Supplementary Fig. 2d, e).** Importantly, we also found that more

134   *Salmonella* were targeted by itaconate in hMDM with the treatment of Su3118, detected

135   by using itaconate biosensor **(Fig. 2e)**. Furthermore, administration of Su3118 in WT mice

136   or administration of AZD3965 in *Mct4*^{-/-} mice significantly promoted the accumulation of

137   intracellular itaconate in the spleen, leading to the detection of higher levels of itaconate

138   by itaconate biosensor in *Salmonella* **(Fig. 2f, g)**. As a result, a lower bacterial load was

139   detected in spleen from mice with MCT1 and MCT4 impairments shown in Fig. 1n.

140   However, in macrophages infected with *Salmonella* Typhi for a shorter period (~7 h),

141   Su3118 failed to modulate the level of the intracellular itaconate **(Fig. 2h)**. This may

142   explain why the percentage of itaconate-targeted *Salmonella* Typhi at around 7 h

143   changed modestly in RAW264.7 cells with MCT1 and MCT4 deficiency **(Fig. 2i)**. In

144   consequence, the replication of *Salmonella* in RAW264.7 cells with the weak activity of

145   MCT1 and MCT4 was strongly inhibited at late but not early (~7 h) time-point of infection

146   **(Fig. 1 and Supplementary Fig. 2f, g)**. Considering a lower proportion of itaconate was

147   secreted at 7 to 8 h post-infection **(Fig. 1c)**, it is predictable that the effect of the inhibitors

148   on itaconate concentration or *Salmonella* killing in the initial phase of infection is rather

149   limited. With the extension of infection, the proportion of secreted itaconate is larger **(Fig.**

150   **1c)**. So, in the later period, MCT1 and MCT4 inhibitors effectively control the secretion of

151   itaconate, leading to increased cellular itaconate and also the attenuated growth of

152   bacteria. To see the influence of MCT1 and MCT4 deficiency on the protein level of IRG1,

153   we analyzed whether the protein level of IRG1 was upregulated by the inhibitors. The

154   results have shown that these inhibitors did not change IRG1 protein level **(Fig. 2j and**

155   **Supplementary Fig. 2h)**. The double deficiency of MCT1 and MCT4 also did not raise

156   the IRG1 protein level **(Fig. 2k)**.

157

158   Given itaconate also has a role in regulating lysosomal biogenesis[8], we measured that

159   whether blocking MCT1 and MCT4 affected lysosomal gene expression. LPS activated

160   the expression of lysosomal genes **(Supplementary Fig. 2i)**. Su3118, the MCT1 and

161   MCT4 inhibitor, hardly regulated the expression of the lysosomal genes **(Fig. 2l)**. Su3118

162   also did not affected the protein level of Lamp1 **(Supplementary Fig. 2j)**. Overall,

163   blocking MCT1/4 probably did not boost the expression of lysosomal genes.

164

165   It is possible that macrophage polarization participate in itaconate-based antibacterial

166   effect[8]. Blocking MCT1 and MCT4 had minimal impact on the polarization of

167   macrophages under during bacterial infection (**Fig. 2m**). Representative flow plot from

168   BMDMs were shown **(Supplementary Fig. 2k)**. Furthermore, the polarization of the

169   majority of macrophages under LPS/IL4 stimulation were not influenced by the inhibition

170   of MCT1 and MCT4 **(Fig. 2n)**. Su3118 also did not significantly change the mRNA level

171   of *Cd206* or *Cd86* in macrophages in response to bacterial infection or LPS/IL4 treatment

172   **(Supplementary Fig. 2l)**. These data suggest that the inhibition of MCT1/4 does not

173   change M1/M2 polarization of macrophages.

174

175   We next also ruled out that the antibacterial immunity was attributed to the effect of lactate,

176   pyruvate, or succinate, which were reported to be transported by MCT1/4. These

177   metabolites showed no antibacterial activity **(Supplementary Fig. 3a-c)** as

178   documented[44-46]. Therefore, our findings indicate that the inhibition of MCT1 and MCT4

179   increases the general amount of itaconate intracellularly, and naturally enhances the

180   antibacterial efficacy of itaconate by promoting the prevalence of itaconate-targeted

181   *Salmonella*.

182

MCT1 and MCT4 transport intracellular itaconate out of cells

To see whether MCT1 and MCT4 transport itaconate out of cells, we have developed an efficient assay to examine itaconate secretion **(Fig. 3a and Supplementary Fig. 2c)**, based on an itaconate biosensor as delineated[13]. We have proved that the eGFP-biosensor of itaconate showed competence in detecting itaconate secretion of LPS-activated RAW264.7 cells **(Supplementary Fig. 4a, b)**, which also indicated that itaconate was released from macrophages in a time- or dose-dependent manner. The data from the LC-MS analysis showed that itaconate was released in a similar pattern **(Supplementary Fig. 4c, d)**. The cell supernatant from same pools of cells was tested separately by LC-MS or itaconate biosensor **(Supplementary Fig. 4e)**. The comparable results underscored the reliability and accuracy of our assays **(Supplementary Fig. 4e)**. And according to our assay, when the simultaneous inhibition of MCT1 and MCT4 activity occurred, the amount of secreted itaconate decreased robustly **(Fig. 3b and Supplementary Fig. 4f)**. Su3118, compared to other MCT1/4 inhibitors AZD3965, VB124, AZD0095 or AR-C155858, showed a clear dose-dependent inhibition on the secretion of itaconate **(Fig. 3c and Supplementary Fig. 4g-j)**. We then also evaluated the MCT1 and MCT4-related effect on itaconate concentration by LC-MS. In HEK 293T cells stably expressing IRG1, overexpression of MCT1 and MCT4 synergistically lowered intracellular itaconate but increased the amount of itaconate in cell supernatant **(Fig. 3d, Supplementary Fig. 4k)**. The inhibition of MCT1 and MCT4 by Su3118 impaired the release of itaconate in RAW264.7 cells **(Fig. 3e)**. Spontaneously, this inhibition led to increasing itaconate in RAW264.7 cells **(Fig. 3f)**. Similarly, in hMDM, itaconate transport is tightly related to MCT1 and MCT4 transport activity **(Fig. 3g, 3h)**. In *Mct1*^{-/-}*Mct4*^{-/-} RAW264.7 cells, the amount of itaconate also increased intracellularly and decreased in extracellular space **(Fig. 3i, j and Supplementary Fig. 4l)**. Importantly, similar results were obtained when treating *Mct4*^{-/-} BMDMs with AZD3965 or WT BMDMs with Su3118 **(Fig. 3k, l and Supplementary Fig. 4m)**. The administration of Su3118 in mice also attenuated the secretion of itaconate into the serum or peritoneal lavage supernatant **(Supplementary Fig. 4n, o)**. These data suggested the important roles of MCT1 and MCT4 in transporting itaconate. These data also indicated that the elevated itaconate levels in cells did not lead to increased extracellular itaconate **(Fig. 3e, j, k)**. If the increase in intracellular itaconate results from an upregulated itaconate production rather than a

215　diminished itaconate secretion, more itaconate should have been detected extracellularly.

216　But less itaconate was identified in the supernatant of cells with the compromised MCT1

217　and MCT4 activity. We further found that the defect in MCT1 and MCT4 still maintained

218　the level of intracellular itaconate-targeting bacteria even when the production of

219　itaconate was damaged by an IRG1 inhibitor (IRG1-IN-1) (**Fig. 3m**). These data along

220　with Figures 2i, 2j indicated that the high level of intracellular itaconate originates from

221　impaired itaconate secretion caused by deficient MCT1 and MCT4 but not enhanced

222　itaconate production. Given that ABCG2 serves as an exporter of itaconate at plasma

223　membrane, we examined the effect of inhibition of ABCG2, MCT1 and MCT4 on itaconate

224　export. We found that the suppression of MCT1 and MCT4 exerts a more significant

225　influence on itaconate release compared to that of ABCG2 when employing Su3118 or

226　KO143 (an ABCG2 inhibitor) at equivalent concentrations. Importantly, the inhibition of

227　ABCG2, MCT1 and MCT4 synergistically block the release of the majority of itaconate

228　from macrophages **(Supplementary Fig. 5a-c)**. Collectively, these findings have strongly

229　supported that MCT1 and MCT4 are exporters of intracellular itaconate.

230

MCT1 and MCT4 transport extracellular itaconate into cells

232　SLC proteins function as bidirectional transporters depending on the concentration

233　gradient of substrates[23]. We next investigated whether MCT1 and MCT4 also transport

234　extracellular itaconate into cells using itaconate biosensor **(Fig. 4a)**. To avoid the

235　interference of endogenous itaconate, we examined itaconate entry in *Irg1*^{-/-} cells or HeLa

236　cells, which lack endogenous IRG1 **(Supplementary Fig. 1i, 6a)**. The MCT1 and MCT4

237　inhibitors Su3118 **(Fig. 4b, c)** or AZD3965+VB124 **(Supplementary Fig. 6b, c)** obviously

238　impaired itaconate uptake into *Irg1*-deficient cell lines. Interestingly, we found that

239　itaconate in the cell supernatant of activated RAW264.7 cells or DC2.4 cells was capable

240　of entering HeLa cells (**Supplementary Fig. 6d**). And Su3118 or AZD3965+VB124

241　hindered itaconate uptake into HeLa cells **(Supplementary Fig. 6e)**. The genetical

242　ablation of MCT1 and MCT4 also impaired itaconate uptake into macrophages **(Fig. 4d)**.

243　Furthermore, less itaconate uptake caused by inhibiting MCT1 and MCT4 transport

244　activity attenuated the effect of itaconate on an oxidative-stress regulator NRF2 (**Fig. 4e,**

245　**f**). NRF2 has been reported to be upregulated by itaconate[16] and has a positive role in

246 resisting bacterial infection[47,48]. This implies that itaconate imported by MCT1 and MCT4

247 also participates in NRF2-dependent antibacterial immunity in cells. More specifically, we

248 utilized ^{13}C-labelled itaconate to assess itaconate uptake into BMDMs. We found that

249 Su3118 inhibited the uptake of ^{13}C-itaconate in a dose-dependent manner in BMDM cells

250 derived from WT or *Irg1*-deficient mice **(Fig. 4g)**. Considering MCT1 and MCT4 are also

251 responsible for transporting lactate, succinate and pyruvate, we scrutinized the impact of

252 these substrates on itaconate transport. We observed that itaconate inhibited lactate

253 uptake in a dose-dependent manner. Based on this data, around 20 μM itaconate

254 effectively inhibits 50% of ^{13}C-labelled lactate uptake into cells **(Fig. 4h)**. Lactate,

255 succinate, and pyruvate, in contrast to malic acid, also impaired the uptake of itaconate

256 **(Fig. 4i)**. We also constructed plasmids for the inactive mutants of MCT1 and MCT4 as

257 documented for lactate transport[43,49,50]. The results from LC-MS showed that the

258 overexpression of WT MCT1 or MCT4 in cells promoted itaconate transport **(Fig. 4j)**.

259 Furthermore, compared to the MCT1/4 mutants, WT MCT1/4 facilitated more itaconate

260 entry into cells, which subsequently was detected by LC-MS **(Fig. 4k, l)** or itaconate

261 biosensor **(Fig. 4m, n)**. Consistently, WT MCT1/4 enhanced lactate secretion compared

262 to the MCT1/4 mutants **(Supplementary Fig. 6f-k)**. This suggests that itaconate shares

263 transport pathways with lactate, succinate, and pyruvate via MCT1 and MCT4. Taken

264 together, these findings suggest that MCT1 and MCT4 are transporters responsible for

265 itaconate translocation into cells.

266

267 **Itaconate transport through MCT1/4 is pH-dependent**

268 Itaconate is a dicarboxylate with two different ionization status, HITA[-] and ITA[2-] (pK_a 3.85

269 and 5.55)[51]. It will be important to validate whether the variation in protonation states

270 affects itaconate transport. Based on the Henderson-Hasselbalch equation, the

271 percentage of monocarboxylic itaconate increases during intracellular acidification

272 (**Supplementary Fig. 6l**). When stimulating primary macrophages with LPS, we observed

273 a decreased intracellular pH (**Supplementary Fig. 6m**), which was consistent with the

274 previous report[52]. It indicates that bacterial infection causes intracellular acidification and

275 promotes itaconate to transfer to its monocarboxylate form. To further explore whether

276 the ionization status of itaconate impacts its transport, we evaluated itaconate uptake and

277 release under different pH conditions. A culture medium containing pH-adjusted itaconic

278 acid was added to the BMDMs. We observed that more itaconate was transported

279 intracellularly at acidic pH **(Fig. 4o)**. We also examined the effect of pH on endogenous

280 itaconate release by adjusting intracellular pH with EIPA. As intracellular pH increased

281 from 5.2 to 8.2, there was a corresponding decrease in the amount of secreted itaconate

282 **(Fig. 4p)**. Consistently, endogenous itaconate accumulated more intracellularly as pH

283 increased **(Fig. 4q)**. Taken together, these data support that itaconate is mainly

284 transported in its monocarboxylate form through MCT1/4.

285

286 **Validation of itaconate transport by MCT1/4 in *xenopus* oocytes and liposomes**

287 To gain more convincing data to support that MCT1 or MCT4 directly transport itaconate,

288 we have set up a *Xenopus laevis* oocytes-dependent transport assay **(Fig. 5a, b)**, which

289 is widely employed to investigate monocarboxylate transport[26]. Human cRNA

290 (complimentary RNA) of MCT1 or MCT4 was injected into *Xenopus laevis* oocytes and

291 incubated for three days. In the itaconate transport assay, we observed that the oocytes

292 expressing recombinant MCT1 or MCT4 demonstrated enhanced uptake of itaconate **(Fig.**

293 **5c)**. This result indicates that MCT1 or MCT4 transport itaconate directly. We next also

294 reconstructed MCT1/4 proteoliposomes by inserting purified human MCT1 or MCT4

295 protein **(Fig. 5d)** as described[22,53]. The proteoliposomes was imaged by cryo-TEM or

296 ODT-microscopy **(Fig. 5e)**. Elevated levels of itaconate are efficiently transported into

297 liposomes incorporating WT MCT1 or MCT4, but not those with mutant forms **(Fig. 5f, g)**.

298 These data suggest that MCT1 and MCT4 directly transport itaconate.

299

300 **MCT1 and MCT4 transport itaconate into *Salmonella*-containing vacuole**

301 Given that *Salmonella*-containing vacuole (SCV) is developed from the plasma

302 membrane[54], it is possible that MCT1 and MCT4 also are located at SCV and transport

303 itaconate into SCV. To investigate this hypothesis, we first examined whether MCT1 and

304 MCT4 are located at *Salmonella*-containing vacuole. We infected RAW264.7 cells by

305 using *Salmonella* stably expressing mScarlet. MCT1 and MCT4 were detected to be

306 recruited to *Salmonella* **(Fig. 6a, b and Supplementary Fig. 7a, b)**. Moreover, MCT1 and

307   MCT4 bound to intravacuolar *Salmonella* manifested by a SCV-reporter strain

308   **(Supplementary Fig. 7c, d)**[55], which aligns with our prior observation that itaconate is

309   delivered into SCV[13]. These observations suggested that the association of MCT1/4 and

310   *Salmonella* may have a strong link to itaconate transport at SCV. We then continued to

311   investigate the hypothesis that MCT1 and MCT4 transported itaconate into *Salmonella*-

312   containing vacuole. In this study, our earlier data have shown that itaconate concentration

313   as well as the ratio of itaconate-targeted *Salmonella* were intracellularly improved in

314   macrophages following Su3118 treatment **(Fig. 2 and 3)**. So, we next tried to assess the

315   impact of concentrated itaconate within cells on the proportion of bacteria decorated by

316   MCT1/4. According to our random sampling and statistical analysis, Su3118 increased

317   the percentage of MCT1/4-targeted *Salmonella* **(Fig. 6a-6d)**. To validate the necessity of

318   the tight association between MCT1/4 and *Salmonella* in itaconate delivery, we analyzed

319   whether MCT1/4-surrounded *Salmonella* was prone to be targeted by itaconate. We have

320   imaged a random sample of RAW264.7 cells infected by *S*. Typhi carrying itaconate

321   eGFP-biosensor and expressing mScarlet **(Fig. 6e, f)**. Intriguingly, most of bacteria were

322   simultaneously targeted by MCT1/4 and itaconate, which was enhanced by Su3118 **(Fig.**

323   **6g, h)**. And the majority of bacteria decorated by MCT1/4 were targeted by itaconate

324   (**Supplementary Fig. 7e-h)**. Alternatively, for all itaconate-positive bacteria, around 35-

325   40% of them had already been enveloped by MCT1/4 in the control groups treated with

326   DMSO **(Fig. 6i, j)**. Elevating the amount of itaconate by Su3118 triggered a greater

327   number of bacteria (around 60-90%) enveloped by MCT1/4, which were previously

328   untargeted by itaconate **(Fig. 6i, j)**. These data suggest that MCT1 and MCT4 transport

329   itaconate into *Salmonella*-containing vacuole.

330

331   **The MCT1 and MCT4-dependent transport of itaconate into SCV is facilitated by**

332   **RAB32**

333   In consideration of our earlier findings that RAB32, located at mitochondria and SCV[56,57],

334   facilitated the delivery of itaconate into SCV by interacting with IRG1 **(Supplementary**

335   **Fig. 8a)**[13,14], the enzyme responsible for itaconate production, we speculated that RAB32

336   coordinated the MCT1 and MCT4-dependent transport of itaconate. We then examined

337   the association between MCT1/4 and RAB32. According to the co-immunoprecipitation

338   assays, we found that MCT1/4 interacted with RAB32 **(Fig. 7a and Supplementary Fig.**
339   **8b).** Although RAB32 interacts with IRG1 more robustly upon bacterial infection, the
340   association between MCT1/4 and RAB32 has already existed in the absence of bacterial
341   infection **(Fig. 7a and Supplementary Fig. 8a)**, which was not strengthened following
342   *Salmonella* infection **(Fig. 7a)**. More importantly, *Salmonella* typhi was decorated by
343   RAB32 as well as MCT1/4 at the same time **(Fig. 7b, c and Supplementary Fig. 8b, c)**.
344   The co-localization of RAB32 and MCT1/4 probably facilitates the transport of itaconate
345   into SCV. Earlier data have shown that itaconate preferentially targets *Salmonella* strains
346   susceptible to the RAB32-mediated antibacterial effect, such as *Salmonella* Typhimurium
347   △GtgE△SopD2, which lacks GtgE and SopD2. To examine the role of RAB32 in the MCT1
348   and MCT4-dependent transport of itaconate, we utilized *Salmonella* Typhimurium
349   △GtgE△SopD2 to infect RAW264.7cells stably expressing eGFP- MCT1/4. The results
350   from microscopy analysis showed that, compared to *Salmonella* Typhimurium, a higher
351   ratio of *Salmonella* Typhimurium △GtgE△SopD2, which cannot neutralize the
352   antibacterial effect of RAB32-itaconate, were targeted by MCT1/4 **(Fig. 7d, e, f, g)**, which
353   underlines that the involvement of RAB32 in mediating MCT1/4-dependent itaconate
354   transport. Collectively, these data suggest, with assistance from RAB32, MCT1 and
355   MCT4 transport itaconate into *Salmonella*-containing vacuole.

356

Discussion

358   We have discovered that the transport function of MCT1 and MCT4 orchestrates the
359   antibacterial immunity of itaconate. As we depicted in Figure 7h, upon *Salmonella*
360   infection, itaconate generation is catalyzed by IRG1 and then itaconate accumulates
361   intracellularly. MCT4, which protein level is increased upon infection, along with MCT1
362   are located at the plasma membrane as well as *Salmonella*-containing vacuole.
363   Comparatively, itaconate is more concentrated in cell cytosol than in the extracellular
364   space or *Salmonella*-containing vacuole early in the infection. So, more itaconate is
365   transported through MCT1 and MCT4 into *Salmonella*-containing vacuole, which is
366   facilitated by RAB32. Meanwhile, itaconate is transported out of cells through MCT1 and
367   MCT4 as the infection persists. However, the inhibition of MCT1 and MCT4 by
368   Su3118/AZD3965+VB124 generally accelerate itaconate accumulation in the intracellular

369   environment, which largely promotes the ratio of itaconate-targeted *Salmonella* and
370   consequently suppresses *Salmonella* survival in macrophages (Fig. 7h). Overall, our
371   findings have confirmed the significance of modulating MCT1 and MCT4-dependent
372   itaconate transport during bacterial infection. And the antibacterial immunity of itaconate
373   is exaggerated in macrophages defective in MCT1 and MCT4 transport activity. But
374   itaconate accumulation resulting from Su3118 treatment may not be sufficient on its own
375   and may require co-stimulatory signals to modulate lysosomal biogenesis or the
376   polarization of macrophages. And, besides itaconate, other substrates of MCT1 and
377   MCT4, which accumulates intracellularly under Su3118 treatment, probably also
378   contribute to this outcome, which requires further study.

379

380   We have also confirmed that MCT1 and MCT4 transported extracellular itaconate into
381   cells (Fig. 4). The attenuation of the itaconate-related effect was noted when inhibiting its
382   uptake via MCT1 and MCT4, as evidenced by the downregulation of NRF2 expression
383   (Fig. 4e, f). Itaconate, imported through MCT1 and MCT4, may act as an important
384   messenger to activate antibacterial activity or other immune responses intracellularly.
385   Additional research is necessary to comprehensively understand the physiological effect
386   of itaconate transported by MCT1 and MCT4. Besides, although the concentration of
387   itaconate in cell supernatant *in vitro* is not high enough to exert antibacterial activity, it
388   would be not surprising that the secreted itaconate fulfills the antibacterial immune
389   responses *in vivo*. For instance, the intestinal epithelial cells facing bacterial infection may
390   uptake itaconate through MCT1/4 in the intestinal lumen to resist bacteria.

391

392   Comparing the itaconate transport activity of MCT1 and MCT4 (Fig. 3 and Fig. 4), we
393   found that MCT1 and MCT4 are essential for itaconate transport. In contrast to the effects
394   of genetic depletion of MCT1 or MCT4 alone on itaconate transport, the simultaneous
395   depletion of both MCT1 and MCT4 resulted in a more pronounced reduction in itaconate
396   transport. Furthermore, overexpression of either MCT1 or MCT4 enhanced itaconate
397   transport. These data suggest that MCT1 and MCT4 may functionally compensate for
398   each other in itaconate transport under certain condition. Additionally, MCT1 is a widely
399   expressed protein, found in the macrophages as well as various mouse tissues such as

400   spleen, liver, brain, and kidney, while MCT4 is an inducible protein in the macrophages,
401   spleen and liver, but not expressed in the brain and kidney (Fig. 1o, 1p, and
402   Supplementary Fig. 1o). These observations suggest that MCT1 and MCT4 may function
403   differently in the uptake of itaconate across different tissues. Given that both transporters
404   are also known to carry lactate or other related substrates[41,43], their efficiency and
405   specificity for itaconate transport may be influenced by substrate competition, depending
406   on the cellular context and metabolic demands. Their transport activity is probably not
407   fixed but dynamically regulated by the availability of competing molecules. We have
408   discovered that the presence of itaconate attenuated lactate uptake (Figure 4h). And
409   lactate also reduced itaconate uptake (Figure 4i). Since MCT1 has a higher affinity for
410   lactate compared to MCT4[41], it is possible that lactate competition has a greater impact
411   on itaconate transport through MCT1. Further investigations along these lines would be
412   valuable in the future.

413

414   Our finding indicates that the environmental pH affects the transport of itaconate through
415   MCT1 and MCT4. Due to protonation, itaconate exists in different forms:
416   monocarboxylate ($HITA^-$) and dicarboxylate (ITA^{2-})[51]. The ratio of monocarboxylate
417   ($HITA^-$) form is increasing due to the acidification of cells in response to infection[52] and
418   LPS treatment (Supplementary Fig. 6m). This property may contribute to the
419   accumulation of itaconate during the early stage of infection to restrict intracellular
420   bacteria and facilitate the export of excess itaconate for a paracrine signal as cells
421   experience acidification during the late stage of infection. A similar mechanism has been
422   investigated in detail for the dicarboxylate succinate, where pH-gated release of succinate
423   occurs in response to exercise[26].

424

425   The location of MCT1/4 at the cell membrane and cytosolic SCV were detected at the
426   same time (Fig. 5). But little known is about whether the MCT1/4 inhibitors used here are
427   absorbed into cells and directly inactivate intracellular MCT1/4. So far, no experimental
428   data have shown that VB124 and Su3118 are membrane permeable, though AZD3965
429   has been reported to enter cells[58]. According to our data, these inhibitors increased
430   intracellular itaconate concentration in general, which also generally induced itaconate-

derived bactericidal activity. Thus, at least, our study has suggested that the inhibitors of MCT1/4 mainly impair the transport of itaconate across plasma membrane but not SCV.

Importantly, our findings have provided evidence that itaconate transport is a key process in cell-autonomous defense against invading bacteria. Considering itaconate as a vertical metabolite, the discovery of itaconate transporters will also provide important clues for further study in different research fields. Besides, our findings connect the antibacterial responses with MCT1 and MCT4, the well-known druggable targets, which may advance the development of antimicrobial drugs along with the therapeutic potential of itaconate itself. The antibacterial properties of MCT1 and MCT4 inhibitors (i.e. Su3118, VB124+AZD3965) endow them with newfound significance, particularly crucial in the fact of the threat of antibiotic failures in treating bacterial infections.

Acknowledgments

Data availability

All related data are available in the main text, supplementary materials, and auxiliary files. The experiment data that support the findings of this study are available from the corresponding author upon reasonable request. The source data underlying Supplementary Fig. 6 and Tables 1, 2, as well as Supplementary Tables 1–9 are provided as a Source Data file. Source data are provided with this paper.

Author contributions

Conceptualization: M.C.

Methodology: Q.M., C.L., P.C., M.C., X.W., F.L.

Investigation: Q.M., C.L., M.C., Y. Z., Y.C., X. C., B.Z.

Visualization: Q.M., C.L., M.C.

Funding acquisition: M.C.

Project administration: M.C., Q.M.

Supervision: M.C.

Writing-original draft: M.C.

Writing-review & editing: M.C., Q.M.

Declaration of interests

The authors declare no competing interests.
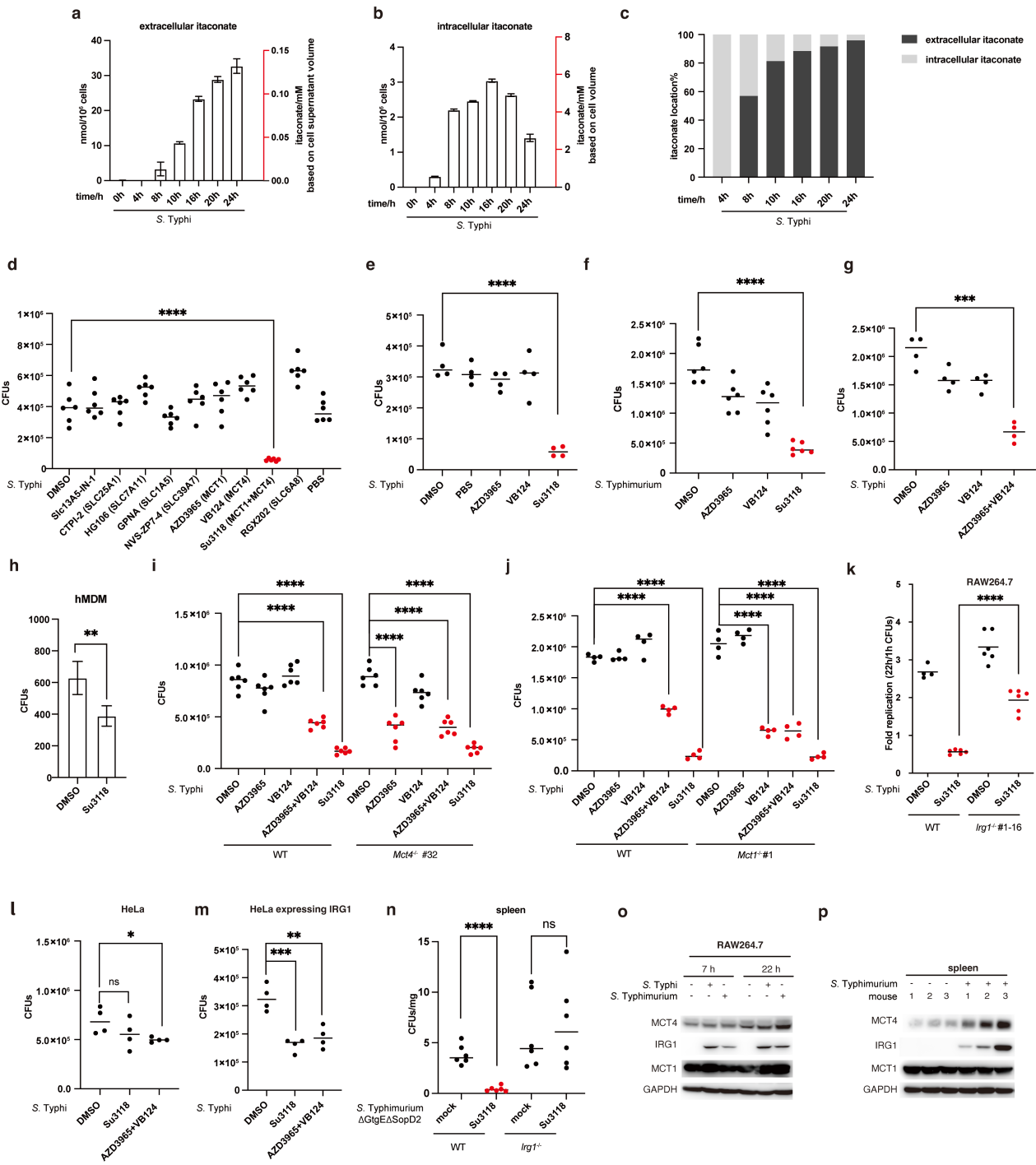
Figures and Figure legends

492

493

494

495

496

497 **Fig. 1 The inhibition of MCT1 and MCT4 transport activity resists *Salmonella***
498 **infection. (a-c)** A larger amount of itaconate is secreted during bacterial infection.
499 Detection of extracellular (a) or intracellular (b) itaconate of RAW264.7 infected by
500 *Salmonella* Typhi (*S*. Typhi, 0, 4, 8, 10, 16, 20, 24 h) by liquid chromatography-mass
501 spectrometry (LC-MS), in which the percentage of itaconate inside and outside of cells
502 was further analyzed (c). **(d)** Su3118 (Syrosingopine, a dual inhibitor for MCT1 and MCT4)
503 inhibits *S*. Typhi growth among various inhibitors. RAW264.7 cells treated with the
504 indicated inhibitors were infected with *S*. Typhi. The number of bacteria in cells was
505 determined at 22 h after infection. Su3118 (10 μM), AZD3965 (1 μM), VB124 (20 μM),
506 RGX-202 (5 μM), GPNA (20 μM), NVS-ZP7-4 (20 nM), SLC13A5-IN-1 (0.044 μM), HG1-
507 6 (5 μM), CTPI-2 (3.5 μM). **(e-g)** The replication of *Salmonella* is obviously attenuated
508 when MCT1 and MCT4 are inhibited at the same time. RAW264.7 cells treated with the
509 indicated inhibitors (Su3118 10 μM, AZD3965 1 μM, VB124 20 μM) were infected with *S*.
510 Typhi (e, g) or *S*. Typhimurium (f) for 22 h. The number of bacteria in cells was examined.
511 **(h)** Human monocyte-derived macrophages (hMDM) treated with DMSO/Su3118 (5 μM)
512 were infected wit*h S.* Typhi for 22 h. The number of bacteria in cells was examined. **(i)** *S.*
513 Typhi shows decreased virulence in *Mct4*$^{-/-}$ RAW264.7 cells treated with AZD3965 (the
514 MCT1 inhibitor, 1 μM). WT (wild-type) or *Mct4*$^{-/-}$ RAW264.7 cells treated with the indicated
515 inhibitors were infected with *S*. Typhi for 22 h. The number of bacteria in cells was
516 determined. **(j)** *S.* Typhi exhibits a reduced ability to grow in *Mct1*$^{-/-}$ RAW264.7 cells
517 treated with VB124 (the MCT4 inhibitor, 20 μM). WT or *Mct1*$^{-/-}$ RAW264.7 cells treated
518 with the indicated inhibitors were infected with *S*. Typhi for 22 h. The number of bacteria
519 in cells was examined. **(k-n)** The deficiency of *Irg1* results in a loss of efficiency for
520 Su3118/AZD3965+VB124 in restricting *Salmonella* proliferation. WT or *Irg1*$^{-/-}$ RAW264.7
521 cells (k), WT HeLa cells (l) or HeLa stably expressing IRG1-Myc (m) treated with the
522 indicated inhibitors were infected with *S*. Typhi for 22 h. The number of bacteria in cells
523 was determined. (n) C57BL/6 (WT) or *Irg1*$^{-/-}$ mice (n=6) were injected Su3118 (5mg/Kg)
524 intraperitoneally. 24 h later, C57BL/6 (wild-type) or *Irg1*$^{-/-}$ mice were infected
525 intraperitoneally with *S*. Typhimurium $\triangle$GtgE$\triangle$SopD2 (10^4 CFU) for 24 h. Bacterial loads
526 in the spleen of the infected mice were analyzed as indicated. **(o, p)** The protein level of
527 MCT4 is enhanced upon infection while the protein level of MCT1 is stable. RAW264.7
528 cells (o) were infected with *S*. Typhi or *S*. Typhimurium for 7 or 22 h. The spleen lysate
529 (p) was collected from mice injected with or without Su3118 (10 μM) and intraperitoneally
530 infected with *S*. Typhimurium (10^2 CFU). The lysates were analyzed by immunoblotting
531 with anti-MCT1, anti-MCT4, anti-IRG1, or anti-GAPDH antibodies. Data in a, b, d-n are
532 mean ± SD from 4-6 replicates. A two-tailed Student's t-test was conducted for pairwise
533 comparisons (h, n), while one-way ANOVA was used for multiple comparisons involving
534 a single independent variable (d-g, i-m). ns, not significant, *p < 0.05, ****p < 0.0001.
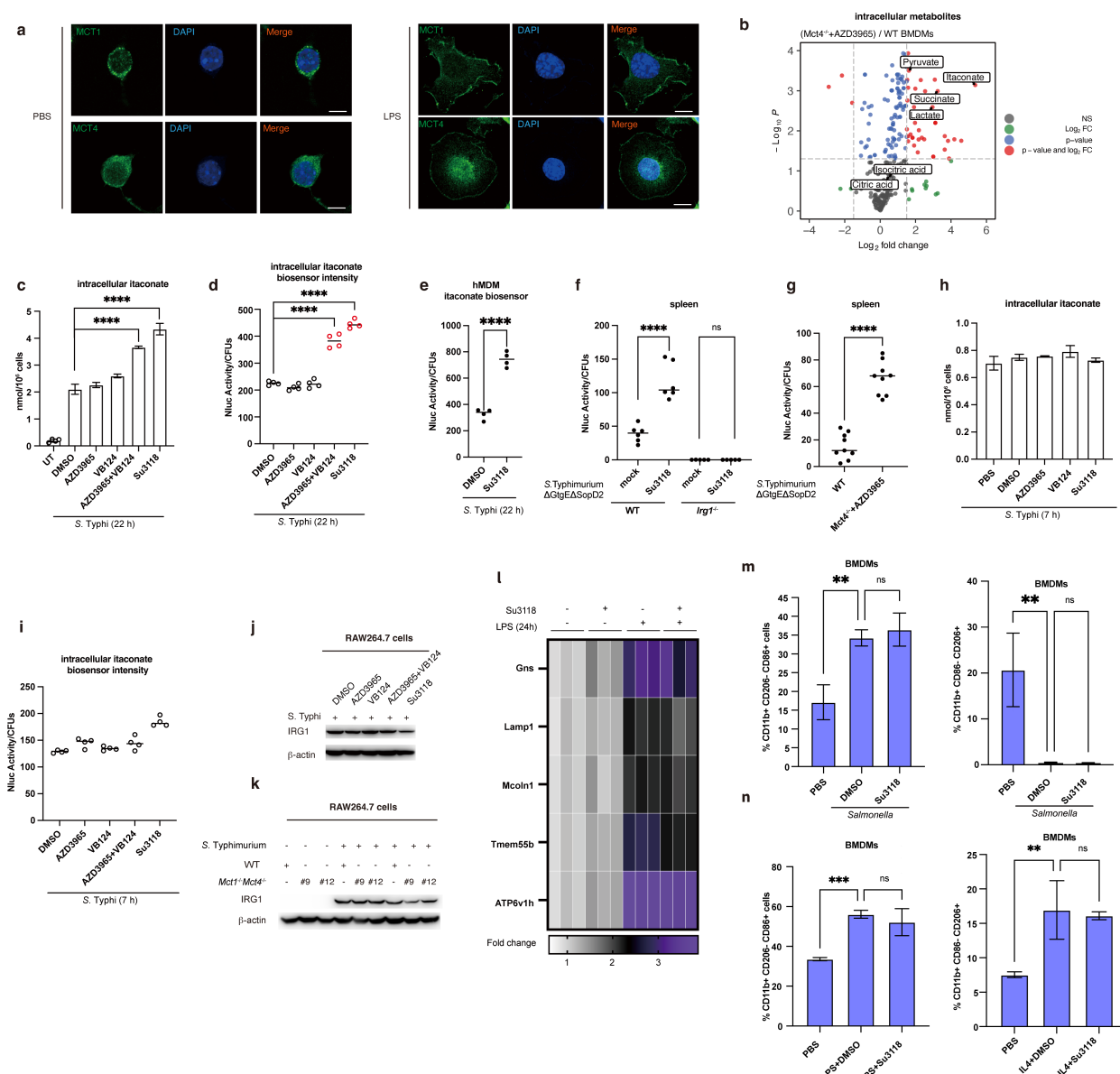
535

536

Fig. 2 The inhibition of MCT1 and MCT4 transport activity promotes the prevalence of itaconate-targeted *Salmonella*. (a) MCT1 or MCT4 is mainly located at the plasma membrane. RAW264.7 cells treated with or without LPS (100 ng/ml) for 24 h were fixed and incubated with MCT1 (Green) antibody, MCT4 (Green) antibody, DAPI (Blue) to visualize nuclei and the related secondary fluorescence antibodies, following an examination under a fluorescence microscope. Scale bar, 10 μm. **(b)** Volcano plot of non-targeted metabolomics from AZD3965-treated *Mct4$^{-/-}$* and WT (wild-type) BMDMs along treated with LPS (100ng/ml). AZD3965, 0, 100 nM. FDR-adjusted p-values were determined by a two-tailed Student's t-test. Red dots indicate significantly changed metabolites (p< 0.05 and Log2 fold change >1.5, n = 6 biologically independent samples in each group). **(c, d)** The intracellular concentration of itaconate is enhanced in cells treated by the MCT1 and MCT4 inhibitors. Intracellular itaconate from RAW264.7 (c, d)

549 treated with the indicated inhibitors (Su3118 10 μM, AZD3965 1 μM, VB124 20 μM) and
550 infected by *S.* Typhi for 22 h were determined by LC-MS or itaconate biosensor. **(e)**
551 Intracellular itaconate from hMDM treated with Su3118 (5 μM), and infected by *S.* Typhi
552 for 22 h were determined by itaconate biosensor. The levels of luciferase were measured.
553 **(f)** C57BL/6 (WT) or *Irg1*$^{-/-}$ mice (n=5/6) were injected with or without Su3118 (5mg/kg)
554 intraperitoneally. 24 h later, mice were infected intraperitoneally with *S.* Typhimurium
555 $\triangle$GtgE$\triangle$SopD2 (10^4 CFU) for 24 h. The levels of luciferase in spleen were measured.
556 **(g)** C57BL/6 (WT) or *Mct4*$^{-/-}$ mice (n=9) were injected with or without AZD3965 (100mg/kg)
557 intraperitoneally. 3 h later, mice were infected intraperitoneally with *S.* Typhimurium
558 $\triangle$GtgE$\triangle$SopD2 (10^4 CFU) for 24 h. The levels of luciferase in spleen were measured.
559 **(h)** RAW264.7 cells treated with the indicated inhibitors (Su3118 10 μM), AZD3965 1 μM),
560 VB124 20 μM) were infected with *S.* Typhi for 7 h. The levels of itaconate in cell lysates
561 were measured. **(i)** RAW264.7 cells treated with the indicated inhibitors (Su3118 (10 μM),
562 AZD3965 (1 μM), VB124 (20 μM)) were infected with *S.* Typhi encoding the
563 nanoluciferase-dependent itaconate biosensor for 7 h. The levels of luciferase in cell
564 lysates were measured. **(j, k)** The impairment of the transport activity of MCT1 and MCT4
565 does not affect IRG1 protein level. RAW264.7 cell (j) treated with the inhibitors (Su3118
566 10 μM, AZD3965 1 μM), VB124 20 μM) were infected with *S.* Typhi for 22 h points. WT
567 or *Mct1*$^{-/-}$*Mct4*$^{-/-}$ RAW264.7 cells (k) were infected with *S.* Typhimurium for 22 h. The cell
568 lysates were analyzed by immunoblotting with anti-IRG1 and anti-β-actin. The levels of
569 luciferase in cell lysates were determined. **(l)** Relative mRNA levels of lysosomal genes
570 in BMDMs treated with Su3118 (5 μM, 24 h), with or without LPS (100 ng/ml, 24 h), were
571 measured by RT-PCR. Expression was normalized to untreated cells, and triplicate
572 values were shown as heatmaps. **(m)** Flow cytometry data from Supplementary Figure
573 2k showing the percentages of CD11b$^+$CD206$^-$CD86$^+$ and CD11b$^+$CD86$^-$CD206$^+$ BMDMs.
574 **(n)** Flow cytometry data from BMDMs treated with Su3118 (5 μM, 24 h), LPS (100 ng/ml,
575 24 h), or IL-4 (20 ng/ml, 24 h), showing the percentages of CD11b$^+$CD206$^-$CD86$^+$ and
576 CD11b$^+$CD86$^-$CD206$^+$ cells. A two-tailed Student's t-test was conducted for pairwise
577 comparisons (e-g, o), while one-way ANOVA was used for multiple comparisons involving
578 a single independent variable (c, d, p). Data in c-l, l-m are mean ± SD from 3-9 replicates.
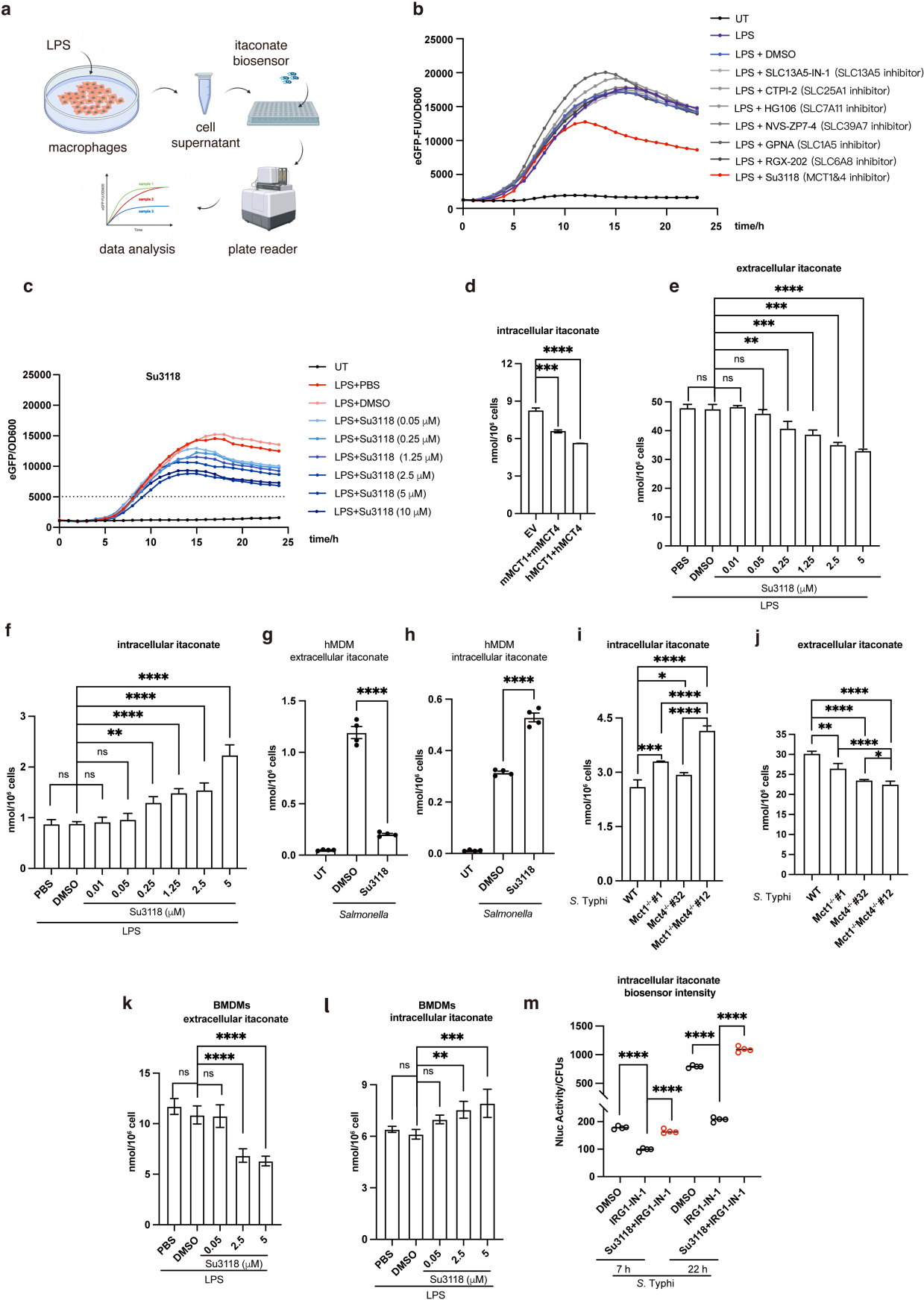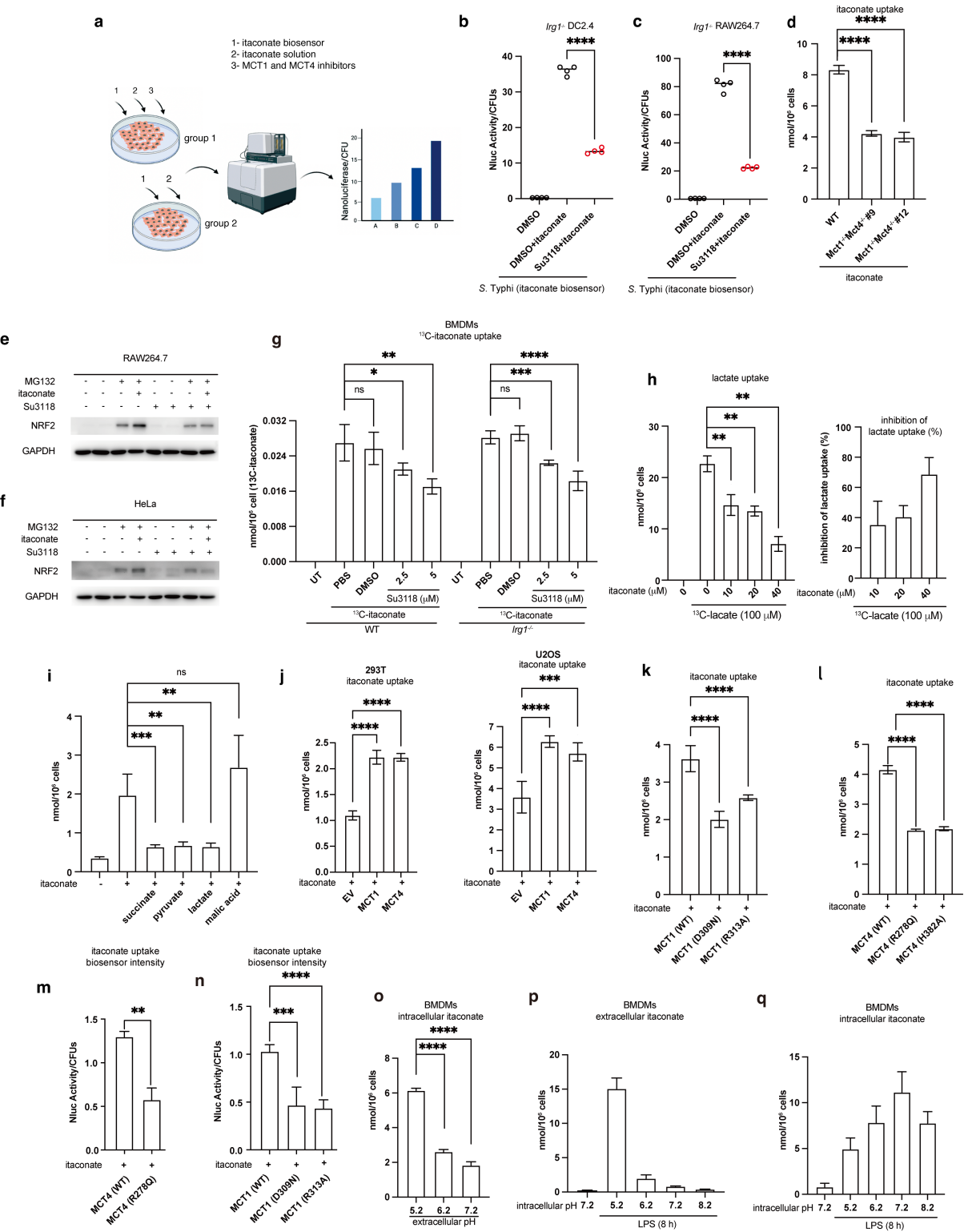579 ****$p < 0.0001$. *$p < 0.05$.

580

Fig. 3 MCT1 and MCT4 transport itaconate out of cells. (a) Development of a biosensor-based assay to detect the secretion of itaconate. **(b, c)** Detection of itaconate in cell supernatant by itaconate biosensor as described in (a). Briefly, RAW264.7 cells stimulated with LPS (100 ng/ml) were also treated with the indicated inhibitors for 24 h. The cell supernatant and *S.* Typhi carrying itaconate eGFP biosensor were mixed and cultured in a 96-well plate. The intensity of eGFP was examined by the plate reader. Su3118 (10 μM), RGX-202 (5 μM), GPNA (20 μM), NVS-ZP7-4 (20 nM), SLC13A5-IN-1 (0.044 μM), HG1-6 (5 μM), CTPI-2 (3.5 μM), VB124 (20 μM), AZD3965 (5 μM) in (b); Su3118 (0, 0.05, 0.25, 1.25, 2.5, 5, 10μM) in (c). **(d)** Detection of itaconate by LC-MS. Intracellular of itaconate from HEK 293T cells stably expressing IRG1 transfected with Flag-MCT1 (h, human; m, mouse), Flag-MCT4 (h, human; m, mouse) were measured by LC-MS. **(e, f)** Intracellular or extracellular of itaconate from RAW264.7 cells treated with LPS (100ng/ml) and Su3118 (the indicated concentrations) for 24 h were determined by LC-MS. **(g, h)** Intracellular or extracellular of itaconate from hMDM treated with Su3118 (5 μM) as well as infected with *S.* Typhi for around 22 h were measured by LC-MS. **(i, j)** Intracellular or extracellular of itaconate from WT, *Mct1*$^{-/-}$, *Mct4*$^{-/-}$, or *Mct1*$^{-/-}$ *Mct4*$^{-/-}$ RAW264.7 cells infected by *S.* Typhi for 22 h were determined by LC-MS. **(k, l)** Intracellular or extracellular of itaconate from WT, *Mct4*$^{-/-}$ BMDMs treated with Su3118(0, 0.05, 2.5, 5 μM) and LPS (100 ng/ml) for 24 h were determined by LC-MS. **(m)** Su3118 restores the level of itaconate in cells with defects in producing itaconate. RAW264.7 cells treated with IRG1-IN-1 and Su3118 were infected with *S.* Typhi encoding the nanoluciferase-dependent itaconate biosensor for 22 h. Data in b-m is mean ± SD from 3/4 replicates. A two-tailed Student's t-test was conducted for pairwise comparisons (g, h). One-way ANOVA was used for multiple comparisons involving a single independent variable (e, f, i-m). *$p < 0.05$, **$p < 0.01$, ***$p < 0.001$, ****$p < 0.0001$. Fig. 3a was created with BioRender.com.

610

611

Fig. 4 MCT1 and MCT4 transport itaconate into cells. (a) Development of a biosensor-based assay to detect itaconate uptake. **(b, c)** The Entry of itaconate into cells is suppressed by Su3118 (a MCT1 and MCT4 inhibitor). $Irg1^{-/-}$ DC2.4 (b) or $Irg1^{-/-}$ RAW264.7 (c) were treated as described in (a). Briefly, $Irg1^{-/-}$ DC2.4 or $Irg1^{-/-}$ RAW264.7 were incubated with itaconate (4 mM), the indicated inhibitors and infected with *S.* Typhi carrying itaconate nanoluciferase biosensor for 22 h. The intensity of nanoluciferase activity was examined by the plate reader. **(d)** WT, $Mct1^{-/-}$, $Mct4^{-/-}$, or $Mct1^{-/-}$ $Mct4^{-/-}$ RAW264.7 cells were incubated with itaconate (4 mM) for 3 h. The uptake of itaconate was measured by LC-MS analysis. **(e, f)** RAW264.7 (e) or HeLa (f) cells were treated with MG132 (10 μM), itaconate (1 mM) or Su3118 (10 μM) as indicated. The cell lysates were analyzed by the immunoblotting with anti-NRF2 and anti-GAPDH. **(g)** WT, $Irg1^{-/-}$ BMDMs were incubated with Su3118 (4 h, 2.5 μM, 5 μM) and ^{13}C-itaconate (2 h, 50 μM). The level of ^{13}C-itaconate was determined by LC-MS. **(h**) $Irg1^{-/-}$ RAW264.7 cells, lack of endogenous itaconate, incubated with itaconate (0-40 μM) and ^{13}C-lactate (100 μM) for 1 hour. The uptake of lactate was measured by LC-MS (Left). Percentage of itaconate inhibiting lactate uptake by analyzing data in the Left (Right). **(i)** BMDMs were incubated with itaconate (0.5 mM), succinate (0.5 mM), lactate (0.5 mM) or malic acid (0.5 mM) for 0.5 hour as indicated. The uptake of itaconate was measured by LC-MS analysis. **(j)** HEK 293T or U2OS cells transfected with EV (empty vector), MCT1, MCT4 were incubated with itaconate (1.5 mM, 1 hour). Itaconate uptake were measured by LC-MS. **(k)** U2OS cells transfected with MCT1 or their mutants were incubated with itaconate (1.5 mM, 1 hour). Itaconate uptake were measured by LC-MS. **(l)** HEK 293T cells transfected with MCT4 or their mutants were incubated with itaconate (1.5 mM, 1 hour). Itaconate uptake were measured by LC-MS. **(m, n)** Itaconate (1 mM, 3h) uptake in HEK 293T cells or HeLa cells transfected with MCT1, MCT4 or their mutants were examined using itaconate biosensor in *Salmonella* Typhi. **(o)** The culture medium's pH was adjusted to 5.2, 6.2 and 7.2, and incubated with BMDMs. Itaconate (1 mM) was incubated with BMDMs for 2 h. The uptake of itaconate was determined by LC-MS. **(p, q)** The intracellular pH of BMDMs was adjusted and maintained at pH levels of 5.2, 6.2, 7.2, and 8.2 using EIPA. BMDMs was also treated with LPS (100ng/ml, 8 h). The level of itaconate was determined by LC-MS. Data in b-d, g-q are mean ± SD from 3 or 4 replicates. **p < 0.01, ***p < 0.001, ****p < 0.0001. A two-tailed Student's t-test was conducted for pairwise comparisons (b, c), while one-way ANOVA was used for multiple comparisons involving a single independent variable (d, g-q). Fig. 4a was created with BioRender.com.
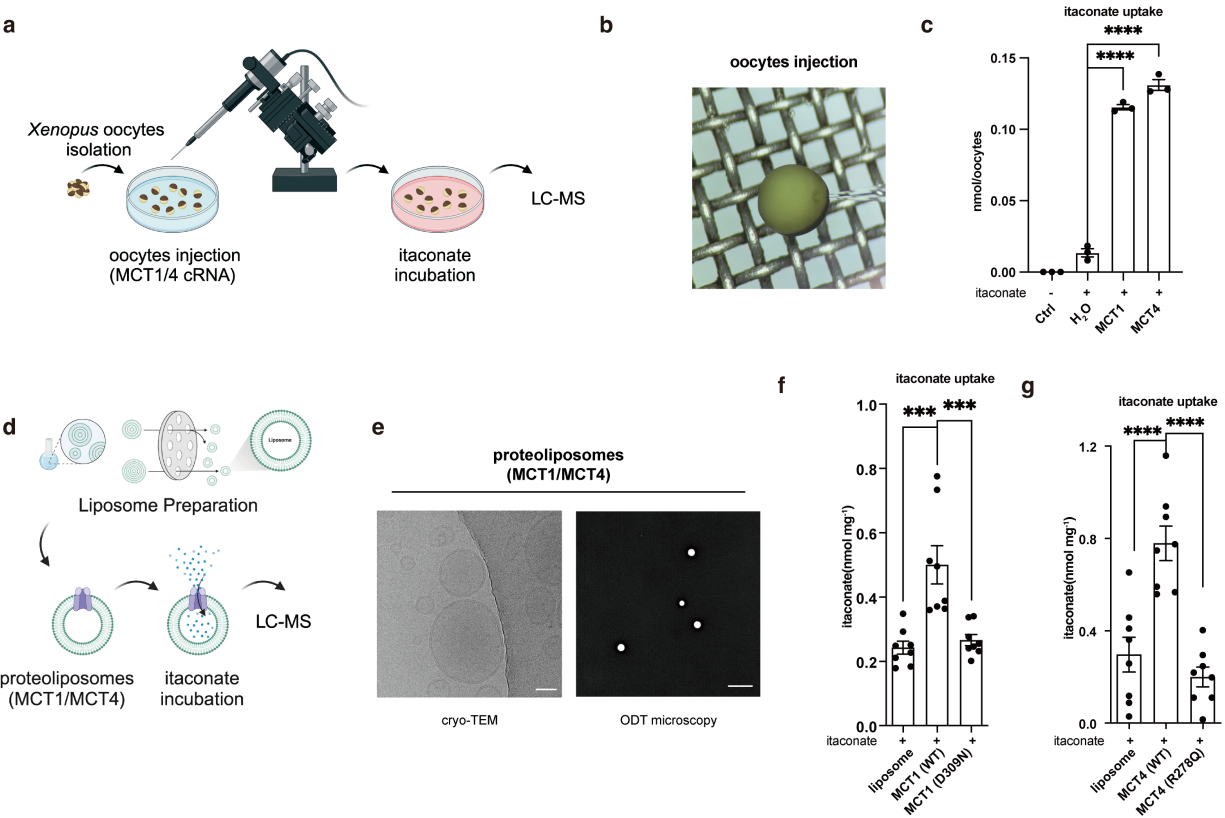
648

Fig. 5 Validation of itaconate transport by MCT1/4 in xenopus oocytes and liposomes. (a) Schematic illustrating itaconate transport into *Xenopus laevis* oocytes mediated by MCT1/4. **(b)** A representative image of a *Xenopus laevis* oocyte during injection. **(c)** Itaconate (1 mM) was incubated with *Xenopus laevis* oocytes expressing human MCT1 or MCT4 for 10 minutes. The uptake of itaconate was measured by LC-MS. **(d)** Schematic illustrating itaconate transport mediated by MCT1/4 into liposomes. **(e)** Images of proteoliposomes were captured from Cryo-TEM (left) and MH-HoliView panoramic super-resolution microscope (right). Scale bars indicated 50 nm and 10 μm, respectively. **(f, g)** The LC-MS analysis of itaconate uptake following the incubation of liposomes reconstituted with MCT1/4 protein and itaconate (1 mM) for 1 hour. The elution buffer containing an equal amount of HA peptides was used to generate control proteoliposomes. Data in c, f, g are mean ± SD from 3 or 8 replicates. ***$p < 0.001$, ****$p < 0.0001$. One-way ANOVA was used for multiple comparisons involving a single independent variable (c, f, g). Fig. 5a, d was created with BioRender.com.
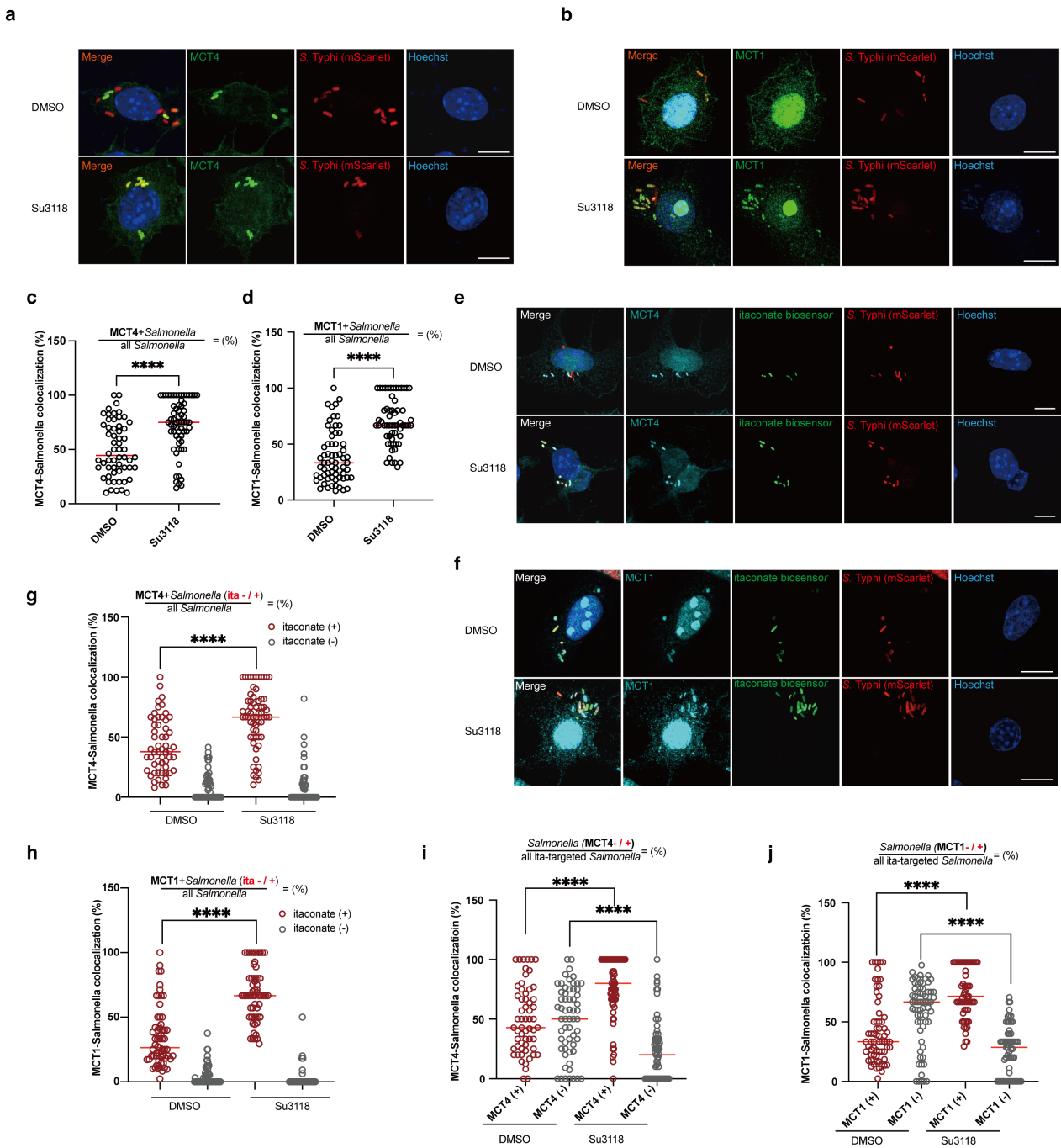
663

664

665

666

667

668

669

670

Fig. 6 MCT1 and MCT4 transport itaconate into *Salmonella*-containing vacuole. (a-d) MCT1/4 targets *Salmonella*, which is augmented by Su3118. RAW264.7 cells treated with DMSO/Su3118 and infected by *S*. Typhi carrying a plasmid encoding mScarlet (Red) for 16 h were fixed, stained with Hoechst (Blue) to mark nuclei, and stained with an anti-MCT1/4 along with Alexa 488-conjugated anti-rabbit antibody (Green), and imaged under a fluorescence microscope. Around 60-70 cells were collected randomly. Representative views of RAW264.7 cells were displayed (a, b). The ratio of bacteria decorated by MCT1/4 in was quantified: $\% = \frac{MCT + Salmonella}{All\ Salmonella}$ (c, d). Each dot represents the ratio of MCT1/4-decorated bacteria within one cell. **(e-j)** MCT1/4 transports itaconate into *Salmonella*-containing vacuole. **(e, f)** RAW264.7 cells treated with DMSO/Su3118 and infected by *S*. Typhi carrying a plasmid encoding mScarlet (Red) and a plasmid encoding itaconate eGFP biosensor (Green) for 16 h were fixed, incubated with Hoechst (Blue) and MCT1/4 antibodies along with Alexa 647-conjugated anti-rabbit antibody (Cyan), and imaged. More than 60 cells were collected unbiasedly. Representative views of RAW264.7 cells were displayed in 5E and 5F. **(g, h)** In each cell, we counted the total number of *Salmonella*, the number of MCT1/4-undecoraed/decorated *Salmonella* (MCT1/4 -/+) and the number of itaconate-untargeted/targeted-*Salmonella* (ita -/+). Then the ratio of itaconate-untargeted/targeted (ita -/+) *Salmonella* (already decorated by MCT1/4) was calculated: $\% = \frac{MCT + Salmonella\ (ita\ -/+)}{All\ Salmonella}$. **(i, j)** The proportion of MCT1/4-undecoraed/decorated *Salmonella* (MCT1/4 -/+) in a pool of itaconate-targeted *Salmonella* was calculated: $\% = \frac{Salmonella\ (MCT\ -/+)}{All\ ita-targeted\ Salmonella}$ .Each dot represents the indicated ratio within one cell. Scale bar, 10 μm. Data in c-d, g-h, i-j are mean ± SD from more than 60 replicates. A two-tailed Student's t-test was conducted for pairwise comparisons (c, d, g, h, i, j). ****p < 0.0001.
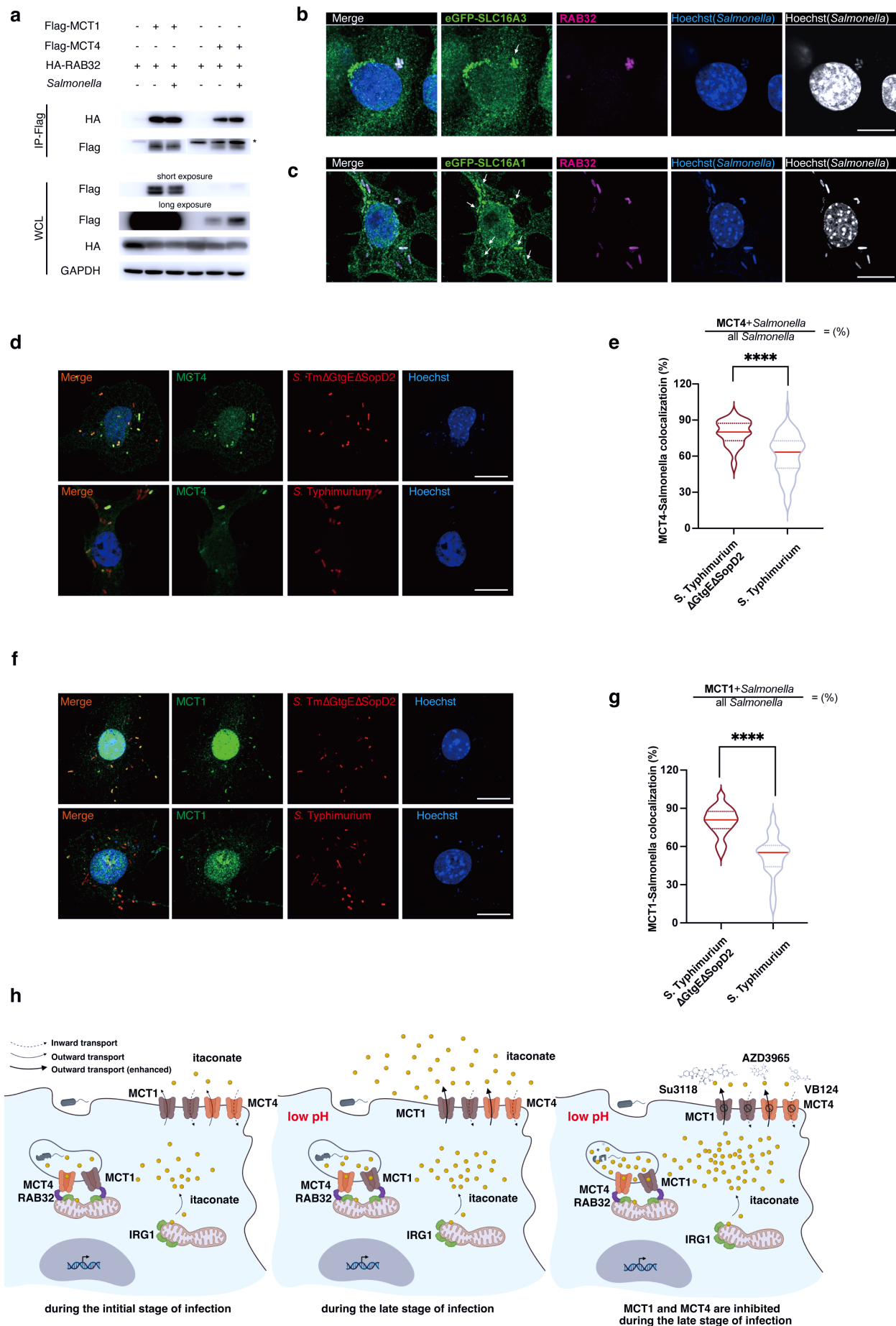
Fig. 7 The MCT1 and MCT4-dependent transport of itaconate into SCV is facilitated by RAB32. (a) RAB32 associates with MCT1/4. HEK293T cells transfected with HA-RAB32, Flag- MCT1/4. The whole cell lysates (WCL) were analyzed by immunoblotting with anti-HA, anti-Flag, or anti-GAPDH antibodies. The interaction of RAB32 and MCT1/4 was examined by the co-immunoprecipation assay. **(b, c)** RAB32 and MCT1/4 synchronously bind to *Salmonella*-containing vacuole. eGFP- MCT1/4 stable RAW264.7 cell lines infected by *S.* Typhi for 22 h were fixed, stained with Hoechst (Blue) and stained with RAB32 (Magenta) antibody along with Alexa 647-conjugated anti-rabbit antibody, and imaged. Scale bar, 10 μM. **(e-g)** *S.* Typhimurium ΔGtgEΔSopD2 is prone to be target by MCT1/4. RAW264.7 cells were infected by *S.* Typhimurium or *S.* TyphimuriumΔGtgEΔSopD2 carrying a plasmid encoding mScarlet (Red) for 22 h and fixed, stained with Hoechst (Blue) to mark nuclei, and incubated with an anti- MCT1/4 along with Alexa 488-conjugated anti-rabbit antibody (Green), and imaged under a fluorescence microscope. More than 60 cells were collected unbiasedly. Representative views of RAW264.7 cells were displayed in 6d and 6f. In each cell, we counted the total number of *Salmonella*, the number of MCT1/4-undecoraed/decorated *Salmonella* (MCT -/+). Then the ratio of MCT1/4-decorated *Salmonella* was calculated: % = $\frac{Salmonella+MCT1/4}{All\ Salmonella}$ (e, g). **(h)** A working model for the mechanism by which MCT1 and MCT4 transport itaconate. MCT1 and MCT4 are responsible for the bidirectional transport of itaconate. And MCT1 and MCT4 are transporters of itaconate at the plasma membrane and *Salmonella*-containing vacuole. RAB32 facilitated the MCT1 and MCT4-dependent transport of itaconate into SCV. Upon *Salmonella* infection, itaconate accumulates in the cell cytosol, and a larger proportion of itaconate is secreted out of cells by MCT1 and MCT4. The impairment of MCT1 and MCT4 transport activity at the plasma membrane highly accelerates itaconate concentration and the ratio of itaconate-targeted bacteria intracellularly, which augments the antibacterial immunity of itaconate (Created with BioRender.com). Scale bar, 10 μM. Data in e, g are mean ± SD from more than 60 replicates. A two-tailed Student's t-test was conducted for pairwise comparisons (e, g). ****p < 0.0001.

732
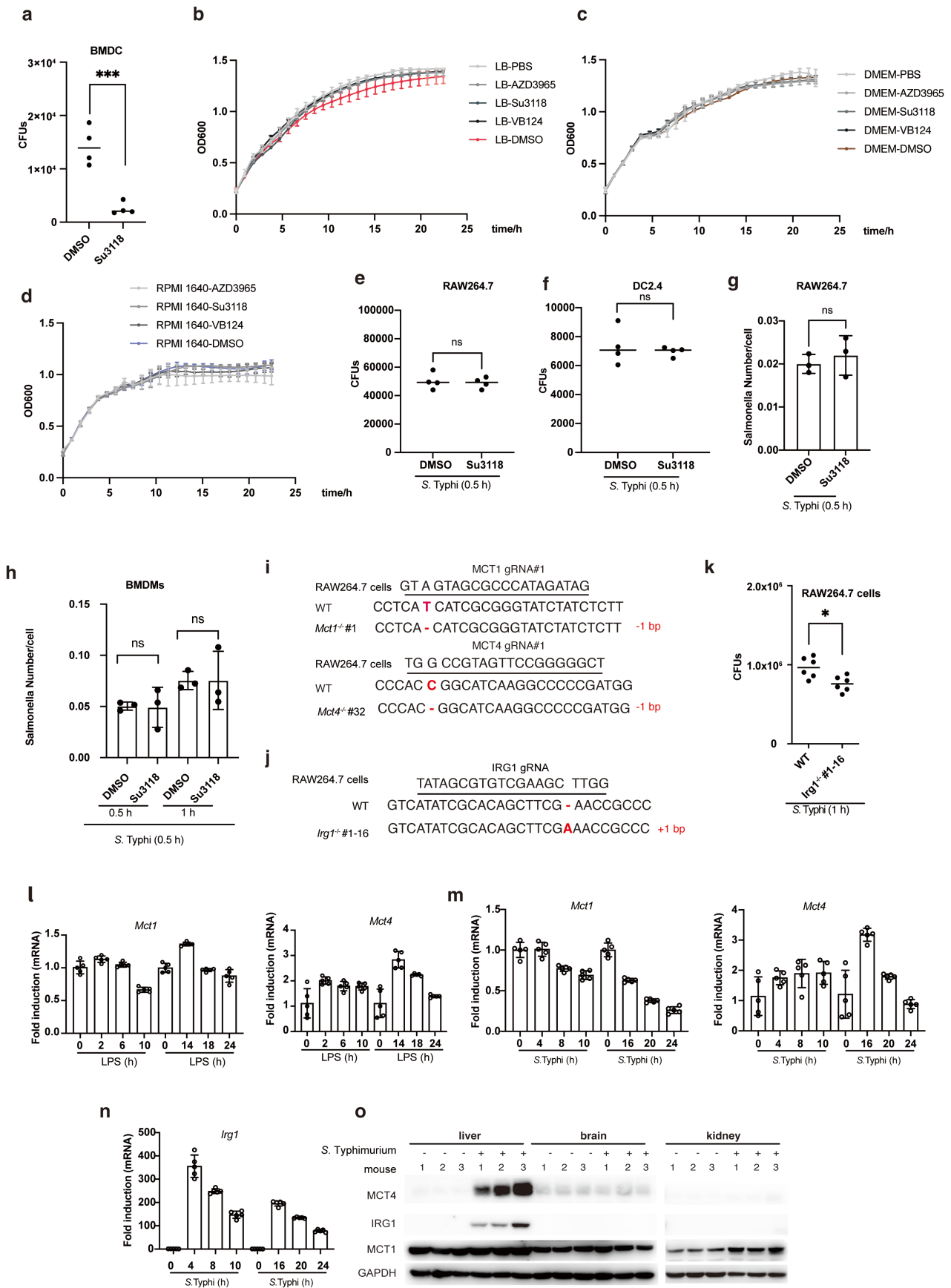
Supplementary Fig. 1 The inhibition of MCT1 and MCT4 transport activity resists *Salmonella* infection. (a-d) The effect of MCT1/4 inhibitors on the growth curve of *Salmonella*. (a) BMDC (bone marrow-derived dendritic cells) treated with the indicated inhibitors were infected with *S*. Typhi. The number of bacteria in cells was determined at 22 h after infection. (b-d) AZD3965, VB124 or Su3118 are the inhibitors of MCT1/4. *S*. Typhimurium was grown in LB media (b), DMEM (c) or RPMI 1640 culture media (d). The growth of *Salmonella* (OD600) was monitored for 24 h by using a microplate reader (The Infinite® M1000-Tecan). **(e, f)** RAW264.7 cells (e) or DC2.4 cells (f) treated with Su3118 (0, 10 μM, 22 h) were infected with *S*. Typhi. The number of bacteria in cells was determined at 0.5 hour after infection. **(g, h)** RAW264.7 or BMDMs pretreated with Su3118 (0, 10 μM, 22 h) were infected with *S*. Typhi stably expressing mScarlet. At the indicated time point, cells were fixed and stained with Hoechst. The number of intracellular *Salmonella* per cell was quantified with Opera Phenix Plus High Content Screening System. **(i)** Sequence alignment analysis of wild-type (WT), *Mct1*$^{-/-}$ or *Mct4*$^{-/-}$ RAW264.7 cells. **(j)** Sequence alignment analysis of wild-type (WT), *Irg1*$^{-/-}$ RAW264.7 cells. **(k)** This is related to Figure 1J. WT or *Irg1*$^{-/-}$ RAW264.7 cells treated with the indicated inhibitors were infected with *S*. Typhi for 1 hour. **(l-n)** Expression of MCT1, MCT4 in cells or mice after LPS treatment or bacterial infection. (l, m) The mRNA level of MCT1, MCT4 or IRG1 in RAW264.7 treated with LPS (l) or infected with *S*. Typhi (m, n) were measured by quantitative real-time PCR. **(o)** Immunoblot analysis of protein extracts from the indicated murine organs with MCT1, MCT4, IRG1 or GAPDH antibodies. Data in a-h is mean ± SD from 3/4 replicates. Data in i is mean ± SD from 6 replicates. Data in j-n is mean ± SD from 5 replicates. A two-tailed Student's t-test was conducted for pairwise comparisons (a, e, f, i). ns, not significant, *p < 0.05. ***p < 0.001.
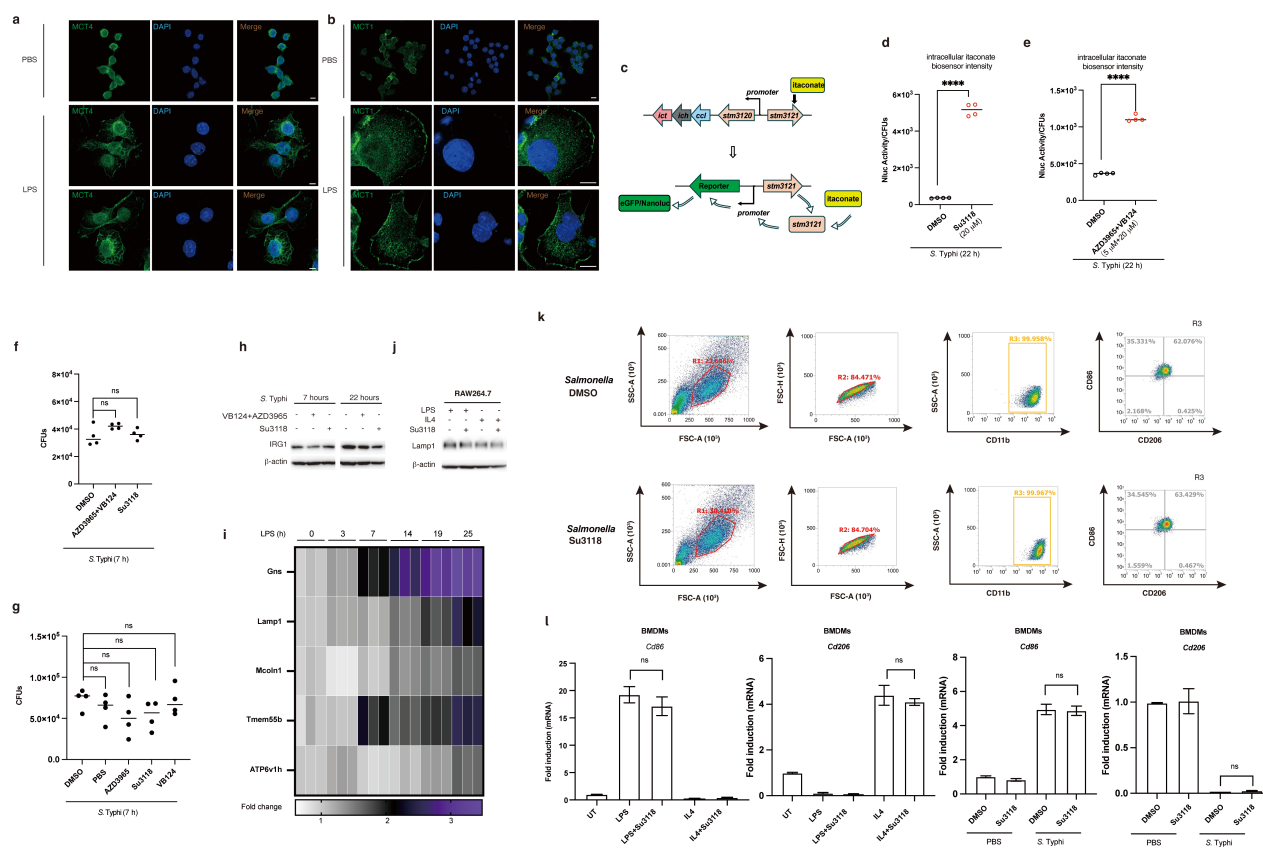
Supplementary Fig. 2 The inhibition of MCT1 and MCT4 transport activity promotes the prevalence of itaconate-targeted *Salmonella*. (a, b) The location of MCT1 and MCT4 in macrophages. RAW264.7 treated with LPS (100ng/ml) for 24 h were fixed, stained with DAPI (Blue) to visualize nuclei and incubated with MCT4 antibody (a) or MCT1 antibody (b) along with Alexa 488-conjugated anti-rabbit antibody (Green), and imaged under a confocal microscope. Scale bar, 10 μm. **(c)** The rationale of itaconate biosensor. **(d, e)** RAW264.7 cells treated with the indicated inhibitors (Su3118 (20 μM), AZD3965 (5 μM) + VB124 (20 μM)) were infected with *S*. Typhi (22 h) encoding the nanoluciferase-dependent itaconate biosensor. The levels of luciferase in cell lysates were measured. **(f, g)** RAW264.7 treated with the indicated inhibitors were infected with *S*. Typhi. The number of bacteria in cells was determined at 7 h after infection. **(h)** Immunoblot analysis of protein extracts from RAW264.7 infected with *S*. Typhi for the indicated time points by using IRG1 and GAPDH antibodies. **(i)** Relative mRNA levels of lysosomal genes in BMDMs treated with Su3118 (5 μM, 24h) with or without LPS (100 ng/ml, the indicated time points) were determined by quantitative real-time PCR. **(j)** RAW264.7 cells treated with LPS (100 ng/ml, 24 h) or IL-4 (20 ng/ml, 24 h). The cell lysates were analyzed by immunoblotting with anti-Lamp1 and anti-β-actin. **(k)** Representative flow plot from BMDMs showing CD11b, CD86, CD206 expression in BMDMs infected with *S*. Typhi (24 h) with or without Su3118 (5 μM, 22 h) treatment. **(l)** Relative mRNA levels of the indicated cytokines in BMDMs treated with Su3118 (5 μM,

780   22 h) with LPS (100 ng/ml, 18 h)/IL-4 (20ng/ml, 18 h) were determined by quantitative
781   real-time PCR. Data in d-g is mean ± SD from 4 replicates. A two-tailed Student's t-test
782   was conducted for pairwise comparisons (d, e, l), while one-way ANOVA was used for
783   multiple comparisons involving a single independent variable (f, g). ns, not significant,
784   ****$p < 0.0001$.
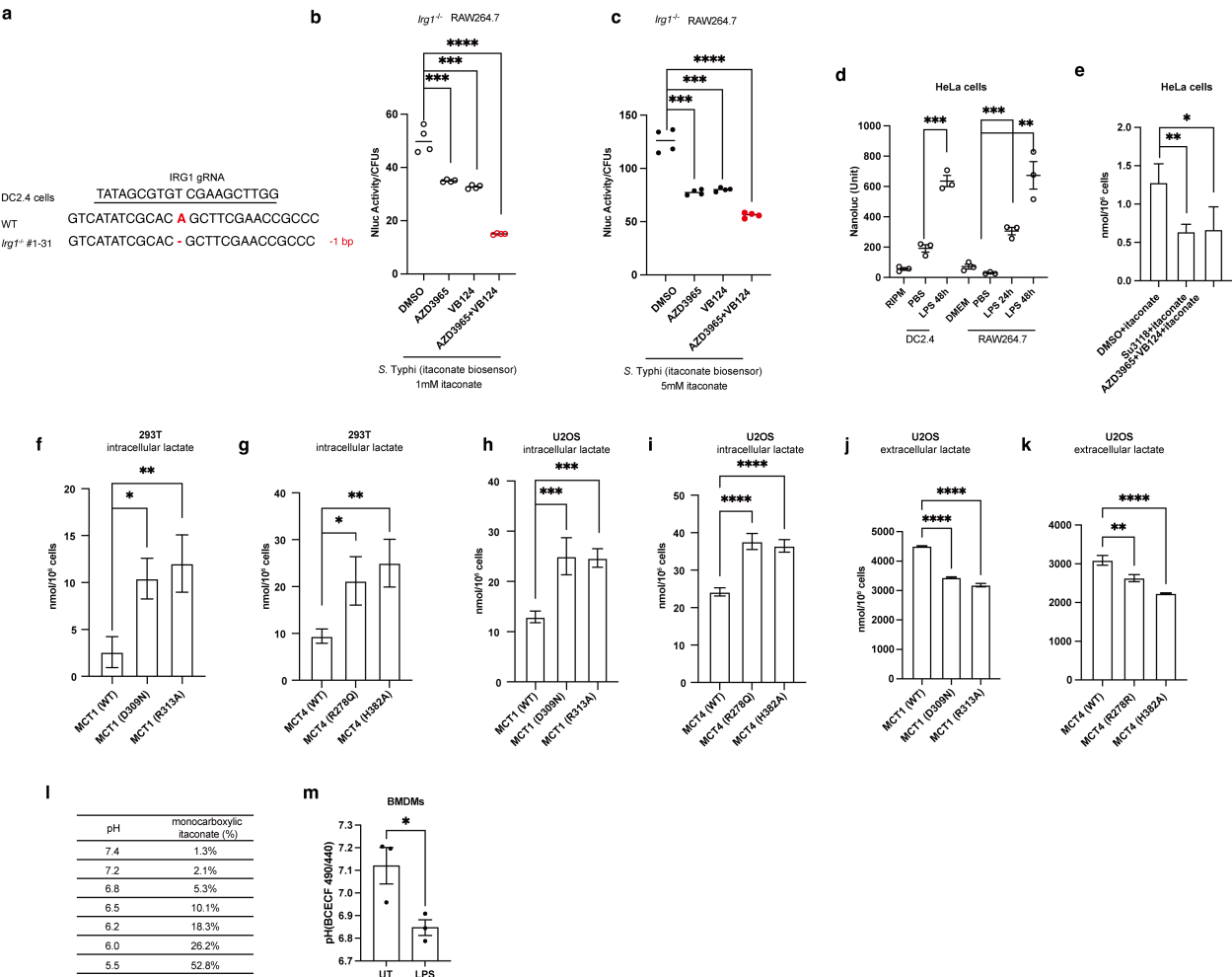
785

786
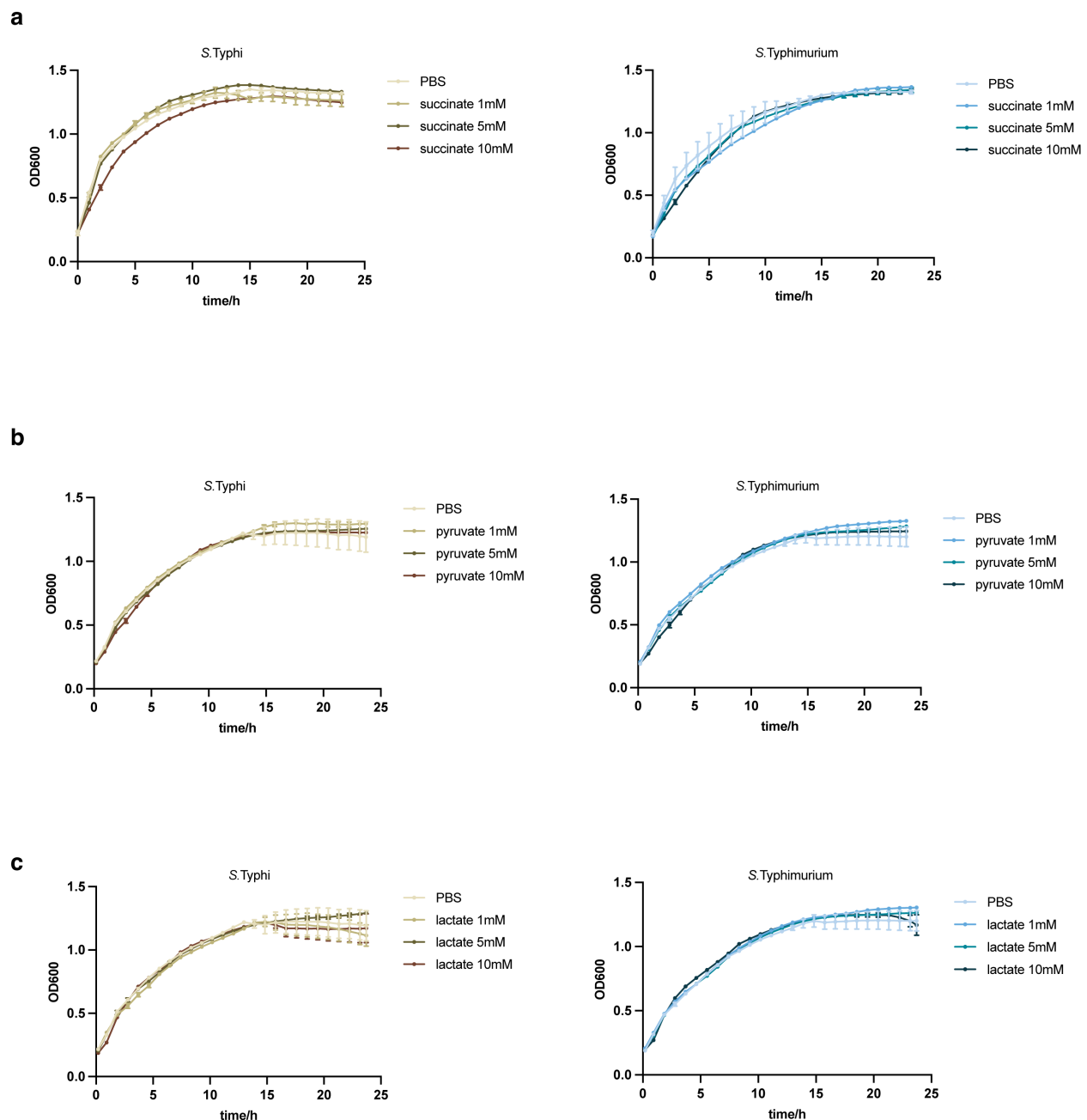
Supplementary Fig. 3 Succinate, pyruvate and lactate do not impair *Salmonella* growth. (a-c) *S*. Typhi or *S*. Typhimurium was incubated in LB containing different metabolites (succinate, pyruvate or lactate) with the indicated concentration. The growth of *Salmonella* (OD600) was monitored for 24 h in a microplate reader. Data in a-c is mean ± SD from 3 replicates.
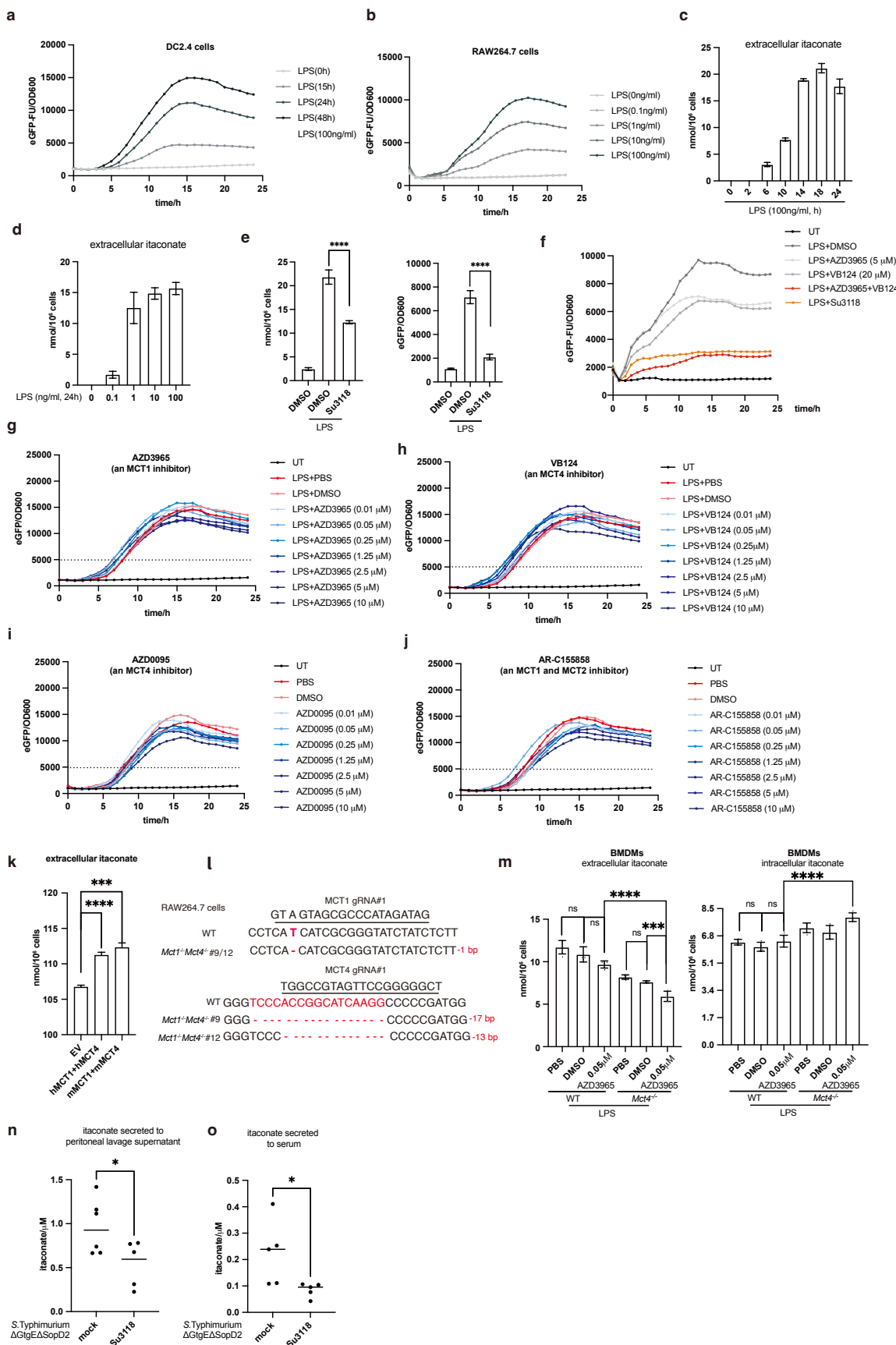
Supplementary Fig. 4 Itaconate secretion is detected by itaconate biosensor or LC-MS. (a, b) Detection of itaconate from cell supernatant by itaconate biosensor. DC2.4 cells (a) were stimulated with LPS (100ng/ml, 0, 15, 24, 48 h). RAW264.7 cells (b) were stimulated with LPS (24h, 0, 0.1, 1, 10, 100ng/ml). The cell supernatant and *Salmonella* carrying itaconate eGFP biosensor were mixed and cultured in a 96-well plate. The intensity of eGFP was examined by the plate reader. **(c, d)** Detection of itaconate from cell supernatant from RAW264.7 cells treated with LPS for the indicated doses or time points by LC-MS. **(e)** Supernatant from same groups of RAW264.7 cells treated with LPS (100ng/ml) and Su3118 (10 μM) were collected and subjected to be analyzed by itaconate biosensor (right) or LC-MS (left). **(f-j)** RAW264.7 cells stimulated with LPS (100 ng/ml) were also treated with the indicated inhibitors (AZD3965, VB124, AZD0095, AR-C155858: 0-10 μM as indicated, VB124 20 μM in fig. f) for 24 h. The cell supernatant and *S.* Typhi carrying itaconate eGFP biosensor were mixed and cultured in a 96-well plate. The intensity of eGFP was examined by the plate reader. **(k)** Detection of itaconate by LC-MS. Extracellular of itaconate from HEK 293T cells stably expressing IRG1 transfected with Flag-MCT1 (h, human; m, mouse), Flag-MCT4 (h, human; m, mouse) were measured by LC-MS. **(l)** Sequence alignment analysis of WT, *Mct1$^{-/-}$ Mct4$^{-/-}$* (#9, #12) RAW264.7 cells. **(m)** Intracellular or extracellular of itaconate from BMDMs treated with AZD3965(0, 0.05 μM) and LPS (100 ng/ml) for 24 h were determined by LC-MS. PBS and DMSO as controls, same groups in Fig. 3i, j. **(n, o)** C57BL/6 (WT) or *Mct4$^{-/-}$* mice were injected Su3118 (5 mg/kg) intraperitoneally. 3 h later, mice were infected intraperitoneally with *S.* Typhimurium △GtgE△SopD2 (10^4 CFU) for 24 h. The levels of itaconate in serum (n=5) or peritoneal lavage supernatant (n=6) were measured by LC-MS. The itaconate level in the peritoneal lavage supernatant represents a relative concentration, determined from 5 ml of PBS used to rinse the mouse peritoneal cavity. Data in a, b, f-j, k is mean ± SD from 3 replicates. Data in c-e, m is mean ± SD from 4 replicates. A two-tailed Student's t-test was conducted for pairwise comparisons (e, n, o), while one-way ANOVA was used for multiple comparisons involving a single independent variable (k, m). *p < 0.05, ***p < 0.001, ****p < 0.0001.

Supplementary Fig. 5 Inhibition of MCT1, MCT4 and ABCG2 abolishes the secretion of the majority of itaconate. (a) RAW264.7 cells infected with *S.* Typhi were treated with the indicated inhibitors (Su3118, 0/10 μM; KO143, 0/10 μM) for 22 h. The levels of secreted itaconate were measured by LC-MS. **(b)** Sequence alignment analysis of WT, *Abcg2*$^{-/-}$ (#1-7, #1-22, #1-28) RAW264.7 cells. **(c)** WT or *Abcg2*$^{-/-}$ RAW264.7 cells stimulated with LPS (100 ng/ml) were also treated with the indicated inhibitors (Su3118, 0, 0.05, 2.5 μM) for 24 h. The cell supernatant and *S.* Typhi carrying itaconate eGFP biosensor were mixed and cultured in a 96-well plate. The intensity of eGFP was examined by the plate reader. Data in a is mean ± SD from 4 replicates. Data in c is mean ± SD from 3 replicates. One-way ANOVA was used for multiple comparisons involving a single independent variable (a). **p < 0.01, ***p < 0.001, ****p < 0.0001.

838

839

Supplementary Fig. 6 MCT1 and MCT4 transport itaconate into cells. (a) Sequence alignment analysis of WT and *Irg1*^{-/-} DC2.4 cells. **(b, c)** The Entry of itaconate into cells is suppressed by the combinational VB124 (a MCT4 inhibitor, 20 μM) and AZD3965 (a MCT1 inhibitor, 1 μM). *Irg1*^{-/-} RAW264.7 incubated with itaconate (1 mM or 5 mM) and treated with the indicated inhibitors were infected with *S.* Typhi carrying itaconate nanoluciferase biosensor for 22 h. The intensity of nanoluciferase activity was examined by the plate reader. **(d)** Itaconate released from LPS-treated DC2.4 or RAW264.7 cells entered HeLa cells. Cell supernatant from RAW264.7 or DC2.4 cells treated with LPS (100ng/ml) or PBS were collected and incubated with HeLa cells for 4 h. Then, HeLa cells were washed with PBS for several times and infected by *S.* Typhi carrying itaconate nano-luciferase biosensor for another 4 h. The levels of luciferase in cell lysates were measured. RPMI 1640 or DMEM media are negative controls. **(e)** HeLa cells were incubated with itaconate (4 mM) and the indicated MCT1/4 inhibitors (Su3118 10 μM, VB124 20 μM, AZD3965 1 μM). The uptake of itaconate were determined by LC-MS. **(f-k)** HEK 293T or U2OS cells were transfected with MCT1, MCT4 or their mutants. 24 h later, the endogenous or extracellular lactate level was measured at 6 h by LC-MS (f-i) or the Lactate-Glo™ Assay (Promega#J5021) (j, k). **(l)** Itaconate exists in both monocarboxylic and dicarboxylic forms at indicated pH, the percentage of monocarboxylic forms was listed according to the Henderson-Hasselbalch equation with pKa = 5.55, PubChem CID 811. **(m)** pH detection with dual-excitation ratiometric pH indicator BCECF-AM (5 μM) in BMDMs with 100ng/ml LPS treatment for 22 h. Data in b-d is mean ± SD from 4 replicates. Data in g is mean ± SD from 3 replicates. A two-tailed Student's t-test was conducted for pairwise comparisons (d), while one-way ANOVA was used for multiple comparisons involving a single independent variable (b-i). *p < 0.05, **p < 0.01, ***p < 0.001, ****p < 0.0001.
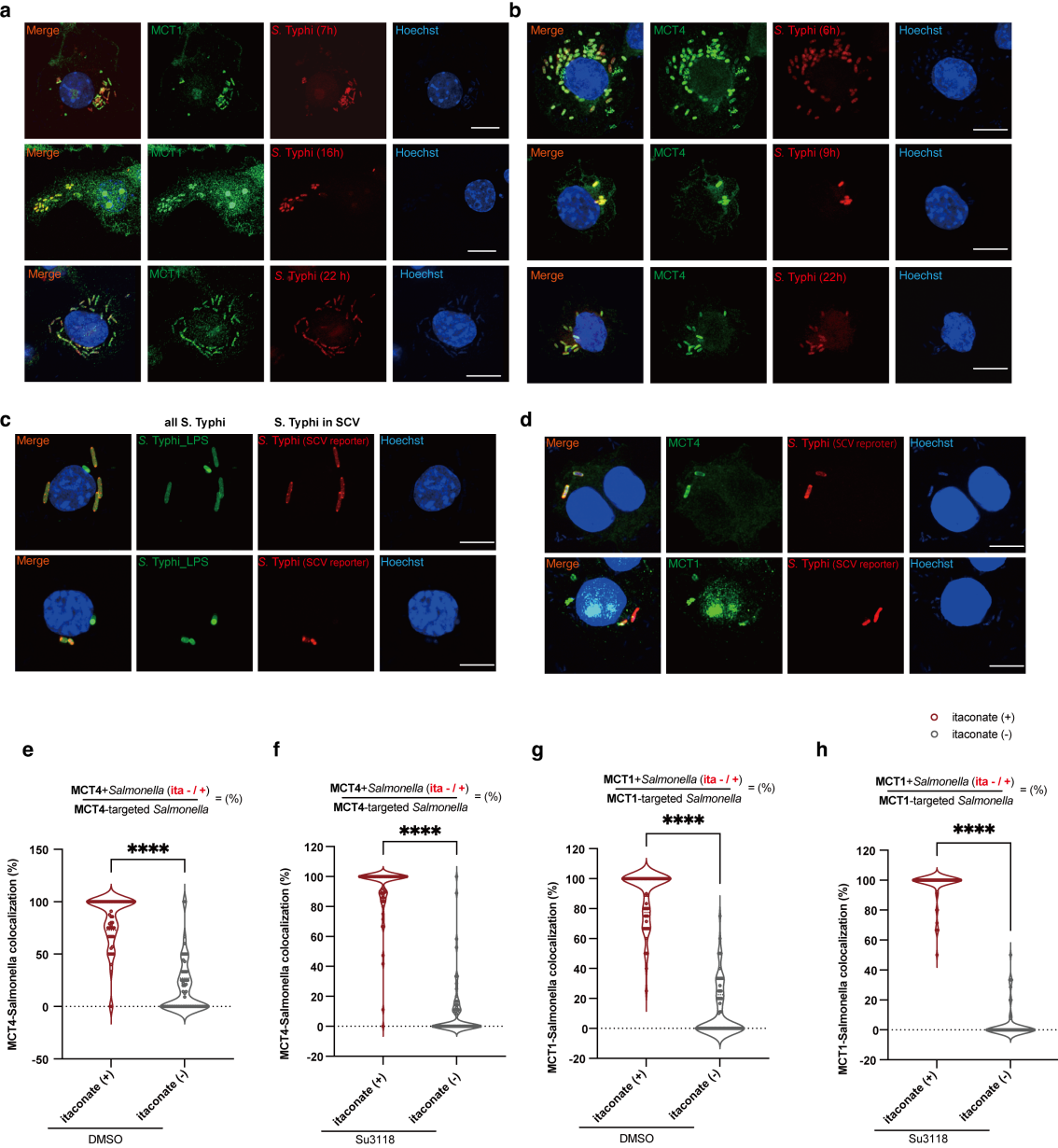
866

867

868

869

870

871

Supplementary Fig. 7 MCT1 and MCT4 transport itaconate into *Salmonella*-containing vacuole. (a-d) MCT1 and MCT4 are co-located with *Salmonella* containing vacuole. **(a, b)** RAW264.7 cells infected with *S*. Typhi expressing mScarlet (Red) for the indicated time points were fixed, incubated with Hoechst (Blue) to visualize nuclei and anti-MCT1/4 along with Alexa 488-conjugated anti-rabbit antibody (Green), and imaged under a confocal microscope. **(c)** The SCV reporter strain *S*. Typhi (SCV reporter) works in cells as described[55]. RAW264.7 cells infected with a SCV reporter strain *S*. Typhi (SCV reporter) (Red) for 3 h were fixed, stained with Hoechst (Blue) to mark nuclei and LPS (Green) to mark all bacteria in the cytosol and SCV. **(d)** RAW264.7 cells infected with a SCV reporter strain *S*. Typhi (SCV) (Red) for 3 h were fixed, stained with Hoechst (blue) and MCT1/4 antibodies (Green). Scale bar, 10 μm. **(e-h)** Itaconate is prone to target MCT1/4-bound *Salmonella*. This is related to Figure 5e and 5f. RAW264.7 cells treated with DMSO/Su3118 and infected by *S*. Typhi encoding mScarlet (Red) and encoding itaconate eGFP biosensor (Green) for 16 h were fixed, stained with Hoechst (Blue) and incubated with MCT1/4 antibodies (Cyan), and imaged. More than 60 cells were collected unbiasedly. In each cell, we counted the total number of *Salmonella*, the number of MCT1/4-undecoraed/decorated *Salmonella* (MCT -/+) and the number of itaconate-untargeted/targeted-*Salmonella* (ita -/+). Then the ratio of MCT1/4-decorated *Salmonella* (ita -/+) was calculated: %$= \frac{\text{MCT} + Salmonella(\text{ita}-/+)}{\text{MCT}-\text{targeted } Salmonella}$. Each dot represents the indicated ratio within one cell. Scale bar, 10 μm. Data in e-h is mean ± SD from 60-70 replicates. A two-tailed Student's t-test was conducted for pairwise comparisons (e-h). ****p < 0.0001.

894
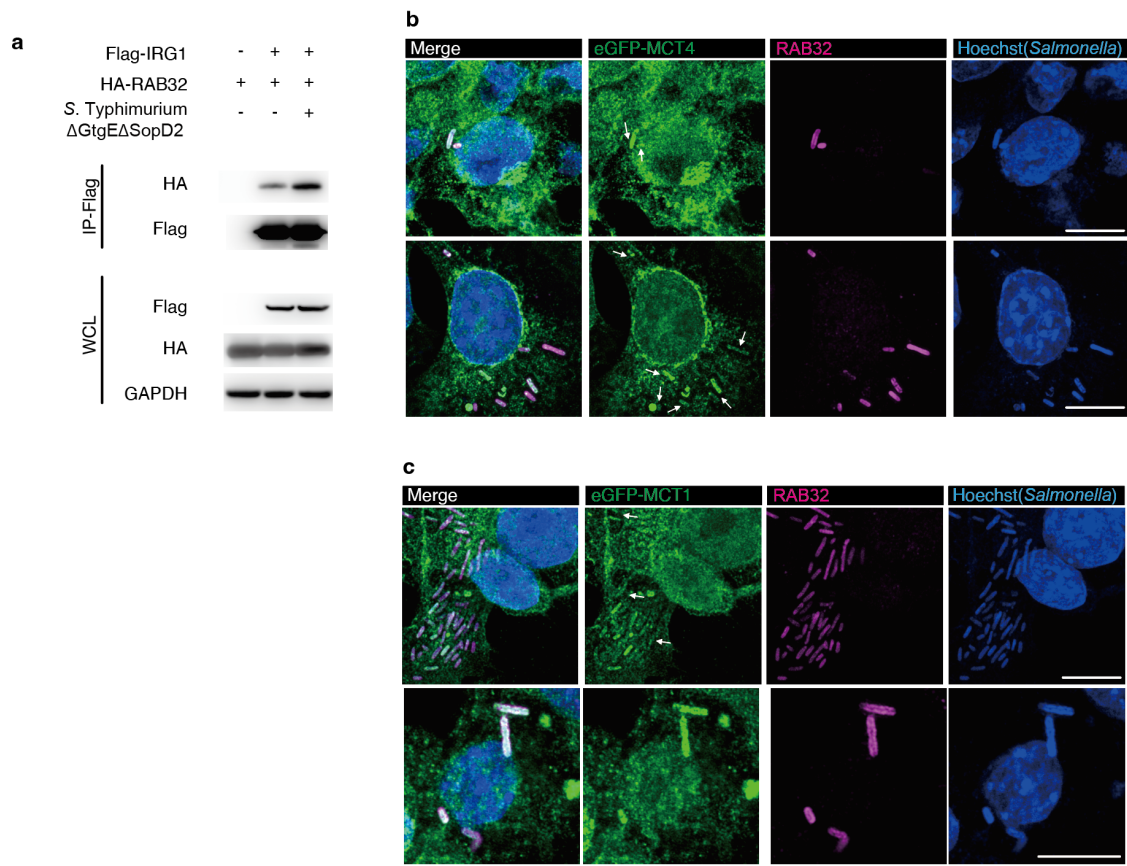
Supplementary Fig. 8 RAB32 and MCT1/4 are co-located at *Salmonella*-containing vacuole. (a) HEK 293T cells transfected with HA-RAB32, Flag-IRG1 (a). The whole cell lysates (WCL) were analyzed by immunoblotting with anti-HA, anti-Flag, or anti-GAPDH antibodies. The interaction of RAB32 and IRG1 (a) was examined by the co-immunoprecipitation assay. The interaction of IRG1 and RAB32 was described in our previous results[13] and also worked as a positive control for this experiment. **(b, c)** eGFP-MCT1/4 (Green) stable RAW264.7 cell lines infected by *S.* Typhi for 22 h were fixed, stained with Hoechst (Blue) to mark *Salmonella* and nuclei and stained with RAB32 (Magenta) antibody along with Alexa 647-conjugated anti-rabbit antibody, and imaged.

904

905

906

907

Methods

Mice. The animal care and experimental protocols underwent thorough review and received the approval from the Institutional Animal Care and Use Committee at Shenzhen Bay Laboratory (SZBL). *Irg1$^{-/-}$* mice (C57BL/6NJ-Acod1<em1(IMPC)J>/J; stock No: 029340) were purchased from The Jackson Laboratory. *Mct4$^{-/+}$* mice (#S-KO-15319) were purchased from Cyagen. *Mct4* homozygous mice were obtained by breeding *Mct4* heterozygous mice (#S-KO-15319) and confirmed through genotyping. LB broth containing *Salmonella* strains were cultured overnight at 37°C and diluted 1:20 in LB supplemented with 0.3 M sodium chloride (NaCl), which then was cultured until reaching an OD600 of 0.9. Intraperitoneal (IP) infection of 8-to-12-week-old animals was carried out using different *Salmonella* Typhimurium strains (CFU as indicated in the figure legends). Mice were administered intraperitoneal injections of Su3118 (5 mg/kg) or AZD3965 (100 mg/kg), as previously documented[36,41,59]. Corn oil (Aladdin #C116025) was utilized as a solvent for both Su3118 and AZD3965, in accordance with the manufacturer's chemical guidelines. Mice receiving intraperitoneal injections of corn oil served as control groups for the Su3118 and AZD3965 treatments. Itaconate in serum or peritoneal lavage supernatant of mice infected was collected and measured as described below. To assess bacterial burdens in the spleens, mice were euthanized at designated time points post-infection, as indicated in the figure legends, and their organs were homogenized in 2 ml of PBS containing 0.05% sodium deoxycholate (0.05% DOC). Subsequent dilutions were plated onto LB agar plates for quantification of colony-forming units (CFUs). To assess the expression of IRG1/MCT1/4/GAPDH, multiple tissue samples from mice were isolated, homogenized, and subjected to subsequent procedures for western blot analysis described below.

932   **Cell culture and Transfection.** RAW264.7 (#SCSP-5036) and HeLa cells (#TCHu187)

933   were obtained from National Collection of Authenticated Cell Cultures. HEK 293T cell line

934   was kindly provided by Professor Gong Cheng (Tsinghua University). DC2.4 cells as

935   kindly provided by Professor Xun Sun (West China School of Pharmacy, Sichuan

936   University). Human monocyte-derived macrophages (hMDM) were kindly provided by

937   Professor Qiankun Wang (Shenzhen Bay Laboratory). Briefly, anonymous human cord

938   blood samples were acquired from MILECELL BIO. To obtain monocyte-derived

939   macrophages, $CD14^+$ cells were cultured for 6-7 days in the presence of 50 ng/ml

940   recombinant human GM-CSF and 50 ng/ml recombinant human M-CSF. The RAW264.7

941   and HeLa cell lines were cultured in Dulbecco's modified Eagle medium (DMEM, GIBCO)

942   supplemented with 10% FBS (#FBS-E500, Newseum) at 37°C with 5% CO2 in a

943   humidified incubator. All cell lines were monthly tested for mycoplasma contamination.

944   BMDC (bone marrow-derived dendritic cells) or BMDMs (Bone marrow-derived

945   macrophages) were isolated from 8-to-12-week-old mice. BMDC or BMDMs were

946   cultured with granulocyte-macrophage colony-stimulating factor (GM-CSF)-containing

947   media or the collected supernatant of L929 cells for around 6-7 days before infection,

948   respectively.

949

950   Mammalian cells were treated with the indicated reagents using the specified working

951   concentrations as below, unless otherwise specified in the figure legends: itaconic acid

952   (4 mM), Su3118 (10 μM), AZD3965 (1 or 5 μM), VB124 (20 μM), RGX-202 (5 μM), GPNA

953   (20 μM), NVS-ZP7-4 (20 nM), SLC13A5-IN-1 (0.044 μM), HG1-6 (5 μM), CTPI-2 (3.5 μM),

954   IRG1-IN-1 (1 mM), MG132 (10 μM), puromycin (2 μg/ml to 10 μg/ml), blasticidin (2 μg/ml

955   to 10 μg/ml). Unless is indicated in the figure legends, pH of all reagent solutions is not

956   adjusted. In a transfection assay, HEK 293T cells were seeded into 6/12/24-well plates

957   and incubated for around 18 h. HEK 293T cells were transfected by following the

958   Lipofectamine 2000 instruction and collected for the indicated analysis in figure legends.

959

960   **Construction of CRISPR/Cas9 Knockout Cell Lines.** The knockout Cell lines were

961   generated by following the CRISPR/Ca9 genetic editing protocol[60]. Simply, pseudotyped

962   virus was generated by co-transfecting pVSVG, △8.9 and lentiCRISPR v2 (gRNA)

963   plasmids at a ratio of 1:2:2, into HEK-293 cells in a 6-well plate by Lipofectamine 2000.

964   Cell culture supernatants were harvested 24 h post-transfection and utilized to transduce

965   the indicated cell lines. Puromycin or blasticidin was used to select and maintain the

966   knockout cell lines. For genotyping of the knockout cell lines, we extracted genomic DNA

967   from cells using a DNA isolation kit (DP304-03, TIANGEN) as DNA templates and

968   subjected to PCR. The PCR products were sequenced and analyzed. Sequences for the

969   gRNAs used are 5'-TATAGCGTGTCGAAGCTTGG-3' for *Irg1*, 5'-

970   GTAGTAGCGCCCATAGATAG -3' for *Mct1*, 5'- TGGCCGTAGTTCCGGGGGCT -3' for

971   *Mct4*. To construct IRG1 or MCT1/4 stable cell lines, similar procedures to those

972   described above were followed. However, pseudotyped virus was generated by co-

973   transfecting pVSVG, Δ8.9, and lenti_CMV_gene into HEK-293 cells in a 6-well plate at a

974   ratio of 1:2:2 using Lipofectamine 2000. Selection and maintenance of the stable cell lines

975   were also achieved using puromycin or blasticidin.

976

977   **Itaconate transport assay in *Xenopus laevis* oocytes.** *Xenopus laevis* oocytes were

978   collected following a well-established protocol[61]. The transport assay was conducted as

979   described[26,61]. Oocytes were injected with MCT1 or MCT4 cRNA (25 ng/oocyte)

980   transcribed from the human MCT1 or MCT4 cloned in the T7-containing plasmid

981   pcDNA3.1 using the mMessage mMachine kit (Thermo Fisher Scientific #AM1344).

982   Oocytes injected with equivalent volume of water acted as our experimental controls.

983   Oocytes were cultured for 3 days in modified Barth's solution (78 mM NaCl, 1 mM KCl,

984   0.33 mM $Ca(NO_3)_2$, 0.41 mM $CaCl_2$, 0.82 mM $MgSO_4$, 2.4 mM $NaHCO_3$, 10 mM HEPES

985   sodium salt, 1.8 mM sodium pyruvate, 10 µg/mL gentamycin, 10 µg/mL streptomycin, pH

986   7.6). To evaluate itaconate uptake, groups of 15 oocytes were incubated in OR2 buffer

987   (2.5 mM NaCl, 2.5 mM KCl, 1 mM $CaCl_2$, 1 mM $MgCl_2$, 1 mM Na_2HPO_4, 5 mM HEPES,

988   pH 6.4) containing itaconate for 10 min. Oocytes were lysed with methanol-acetonitrile-

989   water after they are washed in ice cold OR2 buffer, and subjected to LC-MS analysis, as

990   described below.

991

992   **Liposomes preparation.** Liposomes were reconstituted following a previously described

993   protocol with minor adjustments[22,53]. DOPC, DOPE, and DOPG were mixed in a 1:1:1

994   ratio (20 mg total), and 2 mg of cholesterol was added before dissolving the mixture in 5

995   mL chloroform. The lipids were dried in a rotary evaporator at 40°C with gentle rotation

996   (40 rpm) for 2 h, then re-dissolved in 20 ml dichloromethane and incubated at 30°C for

997   30 minutes in a rotary evaporator. The lipid mixture was dissolved in 50 mM KPi buffer

998   (KH_2PO_4 + K_2HPO_4, pH 7.0) and sonicated at 70 W (2 seconds on, 4 seconds off) for 10

999   min. After three freeze-thaw cycles using liquid nitrogen and liposomes were generated

1000   by extrusion through a 400 nm polycarbonate filter (Whatman Inc.) 11 times using a mini-

1001   extruder (LiposoFast, Avestin Inc.). To ensure complete liposome solubilization, the

1002   suspension was titrated with continuously 10% Triton X-100 at a ratio of 1:500. When the

1003   optical density at 540 nm (OD540) reached its maximum, five additional aliquots of Triton

1004   X-100 were added for complete solubilization of liposomes.

1005

1006   **Proteoliposomes reconstitution.** 40 μg pcDNA3.1-HA-tagged MCT1/4 plasmids were

1007   transfected into EXPI293 (Thermo) or HEK 293T cells in T175 flasks. After 48 h, cells

1008   were lysed in Triton X-100 buffer (50 mM Tris-HCl, pH 7.4, 150 mM NaCl, 5% glycerol,

1009   and 1% Triton X-100), and proteins were enriched using 200 ul Anti-HA Affinity Gel

1010   (Sigma). Following four washes, proteins were eluted by 200 ul of 100 ug/ml HA peptides

1011   (Sigma) in buffer A at 4°C for 1 hour (50 mM KPi, 20% glycerol, 200 mM NaCl, 500 mM

1012   imidazole, 0.05% DDM, pH 7.8). The purified proteins and liposomes were combined at

1013   a 1:100 (wt/wt) ratio. Detergents were removed by incubating the sample with 500 mg/mL

1014   Bio-Beads SM-2 (Bio-Rad) overnight at 4°C, ensuring that air space did not exceed 10%

1015   of the tube volume, and the resulting proteoliposomes were collected from the flow-

1016   through of polyprep columns (Bio-Rad). Finally, the proteoliposomes were concentrated

1017   to 5-10 mg/ml in buffer T (25 mM HEPES, pH 7.5, 150 mM NaCl, and 5 mM $MgCl_2$) by

1018   ultracentrifugation at 270,000 g for 2 h at 4°C with optima XPN-80 (Beckman).

1019

1020   **In vitro Itaconate transport assay.** For the in vitro Itaconate transport assay,

1021   proteoliposomes were incubated with 1 mM itaconic acid in a total of 100 ul buffer T for 1

1022   hour at room temperature. Afterward, the liposomes were washed twice with 1 ml of ice-

1023   cold buffer T, and metabolites inside the liposomes were extracted using 500 ul of

1024   methanol:ACN (1:1). The solvent was then evaporated to dryness at 4°C overnight. The

1025   dried metabolites were dissolved in 30 ul of 50% ACN, and 1 ul of the solution was

1026   analyzed using a QTRAP 6500 LC-MS/MS system.

1027

1028 **Cyro TEM.** Sample preparation for Cryo-TEM was performed using the Vitrobot IV, with

1029 humidity maintained at 100% and the temperature set to 10°C throughout the experiments.

1030 300-mesh copper grids coated with carbon film (Quantifoil® R 1.2/1.3 300 Mesh, Cu)

1031 were glow-discharged using a Pelco EasiGlow unit to render the carbon film hydrophilic.

1032 Then, 3 ul aliquots of the proteoliposomes were applied to each grid, followed by a 10-

1033 second adsorption time. The grid was manually blotted for 3 seconds using Ted Pella

1034 filter paper before being plunged into liquid ethane, which was cooled by liquid nitrogen.

1035 The frozen grids were stored in liquid nitrogen until use. Samples were examined with a

1036 Tundra microscope operating at 100 kV, with an electron dose of 40 electrons/Å for

1037 imaging. Images were captured using a CETA F camera.

1038

1039 **Panoramic super-resolution microscopy.** Proteoliposomes were seeded onto the

1040 glass bottom of 3.5 cm dishes (NEST), and images were captured using optical diffraction

1041 tomography (ODT) with a live MH-HoliView Panoramic super-resolution microscope

1042 (Pellucid Optics Technology, Nantong Co., LTD). The images were then processed using

1043 Fiji software to enhance visualization.

1044

1045 **Bacterial Strains.** *Salmonella* enterica subsp. enterica serovar Typhimurium str. SL1344

1046 was kindly provided by Professor Feng Shao (National Institute of Biological Sciences).

1047 *Salmonella* enterica subsp. enterica serovar Typhi were purchased from National Center

1048 for Medical Culture Collections (CMCC#50071).

1049

1050 ***Salmonella* Genetic Deletion Strains.** *Salmonella* Typhimurium △GtgE △SopD2 was

1051 constructed by using standard recombinant DNA and allelic exchange procedures in

1052 which E. coli SM10 (λπ) acts as the conjugative donor strain. Select merodiploids by

1053 plating diluted bacteria on LB plate containing chloramphenicol (50 μg/ml). The

1054 merodiploids were selected and examined by PCR. One merodiploid was picked and

1055 incubated in LB broth at 37°C for 1 hour. The recombinants were selected on LB agar

1056 plates (no NaCl) supplemented with 10% sucrose at 30°C overnight. The mutant strain

1057 was carefully confirmed by PCR and DNA sequencing and investigated by the infection

1058 procedures.

1059

1060 **Plasmids, Antibodies and Reagents.** All plasmids were constructed by polymerase

1061 chain reaction, restriction enzymes digestion, DNA ligation, or Gibson assembly. The

1062 plasmids used for labelling bacteria were constructed by placing mScarlet into pWSK129

1063 vector. The plasmid for *Salmonella*-containing vacuole (SCV) reporter strain was

1064 constructed by cloning mScarlet and the pltB promoter sequences into pBAD24 vector

1065 referred to a previous study[55]. The plasmid for constructing itaconate biosensor (eGFP or

1066 nanoluciferase) was constructed and prepared according to the previous study[13]. For

1067 detailed plasmid information, please refer to Table S1.

1068

1069 Antibodies used were anti-MCT1 (GXP457728, genxspan; Novus, NBP1-59656), anti-

1070 MCT4 (22787-1-AP, proteintech), anti-IRG1 (19857S, CST), anti-NRF2 (12721S, CST),

1071 anti-β-actin (A1978, sigma), anti-GAPDH (5174S, CST), anti-RAB32 (GTX130477,

1072 Genetex), anti-lamp1 (ab208943, abcam), anti-Flag M2 (F1804, Sigma), anti-HA (26183,

1073 Thermo), Goat anti-Mouse IgG (H+L) Secondary Antibody (C31430100, thermos), Goat

1074   anti-Rabbit IgG (H+L) Secondary Antibody (C31460100, thermos) . 488-conjugated Goat

1075   Anti-Mouse IgG(H+L) (SA00013-1), 488-conjugated Goat Anti-Rabbit IgG(H+L)

1076   (SA00013-2), 594-conjugated Goat Anti-Mouse IgG(H+L) (SA00013-3); 594-conjugated

1077   Goat Anti-Rabbit IgG(H+L) (SA00013-4) antibodies were from proteintech.

1078

1079   Other reagents used in our study are listed below. Itaconic acid was purchased from

1080   Sigma (#I29204-100G). LCMS-grade Acetonitrile (#1.00029.2508) and methanol

1081   (#1.06035.2500) were purchased from Merck. SLC inhibitors Su3118 (S9907), AZD3965

1082   (S7339), VB124 (S9929), RGX-202 (E1223), GPNA (S6670), NVS-ZP7-4 (S6668),

1083   SLC13A5-IN-1 (S0755), HG1-6 (E1080), CTPI-2 (S2968), 5-(N-Ethyl-N-isopropyl)-

1084   Amiloride (EIPA) (S9849) were purchased from Selleck. IRG1-IN-1 (HY-148335) was

1085   purchased from MCE. DAPI (C1002, beyotime) or Hoechst stain (H1398, Thermo) used

1086   for DNA/cell nucleus staining. ^{13}C-labeled itaconate (0.5mg, sc-495554) was purchased

1087   from SANTA. Lipofectamine 2000 (11668019, Thermo) used for transfection. LPS of

1088   bacteria is purchased from Sigma (L2018). GM-CSF (315-03) for culturing BMDC is

1089   purchased from PEPROTECH. Puromycin (ant-pr-1) and blasticidin (ant-bl-05) were

1090   purchased from InvivoGen.

1091

1092   **Biosensor-based Itaconate Detection Assay.** *Salmonella* strains carrying plasmids

1093   encoding the nanoluciferase or eGFP itaconate biosensors were cultured overnight for

1094   around 18 h. To detect itaconate secretion, the overnight culture of *Salmonella* carrying

1095   the eGFP itaconate biosensor were diluted to an OD600 of 0.05 to 0.1 in LB and grown

1096   until the OD600 reaching 0.3. The *Salmonella* cultures were centrifuged and resuspended

1097   into PBS. The mammalian cell supernatant was added to the *Salmonella* cultures, and

1098   seeded into a 96-well plate. The expression of the eGFP was measured by the Tecan

1099   Infinite®M1000 plate reader. To detect the level of intracellular itaconate, the overnight

1100   culture of *Salmonella* carrying the eGFP/nanoluciferase itaconate biosensor were sub-

1101   cultured and infected mammalian cells by following the described bacterial infection

1102   protocol. eGFP was detected by microscope as described in this study. Luciferase

1103   intensity of the itaconate biosensor was measured by using the Nano-Glo® Luciferase

1104   Assay System (Promega) and the Tecan Infinite®M1000 plate reader.

1105

1106   **Measurement of itaconate by LC-MS.** RAW264.7 or other cell types ($\sim 3 \times 10^6$/ml) treated

1107   with indicated stimuli or infected with *Salmonella* were washed with 0.9% NaCl. Samples

1108   were extracted with methanol-acetonitrile-water at 2:2:1 (v/v/v). The standards quality and

1109   controls (QCs) were prepared in control cell extract matrix at the appropriated

1110   concentration range (1-1000ng/ml). The cell extracted samples together with the

1111   standards and QCs were directly injected onto LCMS system for analysis. LCMS analysis

1112   was performed on a QTRAP 6500+ (AB Sciex, Singapore) coupled to an ExionLC AD

1113   Series LC system (Shimadzu, Kyoto, Japan). Analyst software (version 1.7.1, AB Sciex,

1114   Warrington, UK) was used for data acquisition and analysis. A targeted Multiple Reaction

1115   Monitoring (MRM) method was utilized to quantify the level of itaconate. AnACQUITY

1116   UPLC® BEH C18 column (1.7um, 2.1x100mm, P.N.186002352) coupled with InfinityLab

1117   Poroshell 120 EC-CN guard column (2.7 µm, 4.6 x 5 mm, P.N.820750-927) was utilized

1118   for the liquid chromatography separation at 40°C. The gradient started with 98% formic

1119   acid (0.05%) (A) and 2% acetonitrile (B), maintained for 1 min and increased to 95% B in

1120   8 min, maintained for 2 min, then increased to 2% B in 1 min and back to 95% in 1min

1121   and maintained at 2% B for 2 min. The total run time was 15 min. QTRAP 6500+ mass

1122 spectrometer was operated using an electrospray ionization (ESI) source in negative ion

1123 mode. MRM transition monitored for itaconate was 129.0/85.1. The source settings were

1124 as follows: gas temperature of 500 °C, Curtain Gas set to 35, Ion Spray Voltage Floating

1125 set to 4500, Ion Source Gas 1 set to 50, Ion Source Gas 2 set to 50, and ion polarity set

1126 to negative. Data acquisition and analysis were performed using the SCIEX OS software

1127 (version 1.7.0, AB Sciex, Warrington, UK).

1128

1129 **Bacterial Infections.** To infect the indicated mammalian cells, *Salmonella* strains were

1130 cultured overnight at 37°C and diluted 1:20 into LB broth containing high-concentration

1131 NaCl (0.3 M) and grown to an OD600 of 0.9. The multiplicity of infection (MOI) of

1132 *Salmonella* is 5 for *Salmonella* Typhimurium or 10 for *Salmonella* Typhi. Cells were

1133 infected for one hour in Hank's balanced salt solution (HBSS). Cells were then washed

1134 several times with cell culture medium and incubated in culture medium containing

1135 gentamycin (100 µg/ml) to kill extracellular bacteria for one hour. In order to avoid

1136 repeated cycles of infection, cells were then washed and fresh medium containing

1137 gentamycin (10 µg/ml) was added. Cells were incubated for the specified durations as

1138 indicated in the figure legends. The number of intracellular bacteria were determined by

1139 a series of dilution and plating measurable bacteria colonies on agar plates.

1140

1141 **Quantitative PCR.** RNA from mammalian cells was extracted using TRIzol Reagent

1142 (9109, TAKARA), and first-strand cDNA was synthesized from the total RNA employing

1143 oligo-dT primers and reverse transcriptase (RR036A, TAKARA). Real-time PCR was

1144 conducted utilizing the 2×RealStar Green Fast Mixture (A301-1, Genstar) and specific

1145 primers, analyzed with CFX96 Touch Real-Time PCR Detection System. The obtained

1146   data were normalized to the GAPDH gene, and the relative transcript abundance was

1147   determined using the Ct method.

1148

1149   The following primers were utilized for real-time PCR:

1150   mouse *Mct1* forward primer, 5'- TGTATGCTGGAGGTCCTATCAG -3'
1151   mouse *Mct1* reverse primer, 5'- CCAATGCACAAGTAAAGTTCCTG -3'
1152   mouse *Mct4* forward primer, 5'- GCCACCTCAACGCCTGCTA-3'
1153   mouse *Mct4* reverse primer, 5'- TGTCGGGTACACCCATATCCTTA -3'
1154   mouse *Gapdh* forward primer, 5'- GAAGGGCTCATGACCACAGT-3'
1155   mouse *Gapdh* reverse primer, 5'- GGATGCAGGGATGATGTTCT -3'
1156   mouse *Cd86* forward primer, 5' - TCAATGGGACTGCATATCTGCC -3'
1157   mouse *Cd86* reverse primer, 5' - GCCAAAATACTACCAGCTCACT -3'
1158   mouse *Cd206* forward primer, 5' - GAGGGAAGCGAGAGATTATGGA -3'
1159   mouse *Cd206* reverse primer, 5' - GCCTGATGCCAGGTTAAAGCA -3'
1160   mouse *Lamp1* forward primer, 5' - CAGCACTCTTTGAGGTGAAAAAC -3'
1161   mouse *Lamp1* reverse primer, 5' - ACGATCTGAGAACCATTCGCA -3'
1162   mouse *Mcoln1* forward primer, 5' - CTGACCCCCAATCCTGGGTAT -3'
1163   mouse *Mcoln1* reverse primer, 5' - GGCCCGGAACTTGTCACAT -3'
1164   mouse *Tmem55b* forward primer, 5' - TACGGAGCCGGTAAACATGC -3'
1165   mouse *Tmem55b* reverse primer, 5' - GGCTAGTCAAGGGTGAGTAGG -3'
1166   mouse *Gns* forward primer, 5' - TGTGCGGCTATCAGACCTTTT -3'
1167   mouse *Gns* reverse primer, 5' - CAGGGCATACCAGTAACTCCA -3'
1168   mouse *Atp6v1h* forward primer, 5' - TCTGATGACGCACATCTCCAA -3'
1169   mouse *Atp6v1h* reverse primer, 5' - GCTGACACGCTGGTGATTTTC -3'

1170

1171   **Western Blotting and Co-immunoprecipitation Assay**. The mammalian cells or murine

1172   tissue were lysed and extracted by NP-40/RIPA buffer. The protein samples were

1173   denatured and loaded into 8-10% SDS-polyacrylamide gel. The proteins in gel were

1174   subsequently transferred onto polyvinylidene fluoride (PVDF, BIO-RAD, 1620177)

1175   membranes, blocked with 5% (w/v) milk at room temperature for around one hour. PVDF

1176   membranes were incubated with primary antibodies against IRG1, MCT1, MCT4, GADPH,

1177 NRF2 or other indicated targets overnight at 4°C. Following this, the membranes were

1178 further incubated with the secondary antibody, and the blots were visualized using

1179 Amersham ImageQuant 800 Western blot imaging systems.

1180

1181 For immunoprecipitation, whole-cell extracts were collected and subjected to be analyzed

1182 by western blotting. These extracts were then incubated overnight with anti-Flag agarose

1183 gels (A2220, from Sigma). Subsequently, the beads underwent 5-6 washes with low-salt

1184 lysis buffer, and immunoprecipitated proteins were eluted using 2×SDS Loading Buffer

1185 and separated by SDS-PAGE. The samples were further analyzed by western blotting.

1186

1187 **Microscopy.** RAW264.7 or the other indicated mammalian cells were plated on glass

1188 coverslips and incubated overnight. Cells were infected with the indicated *Salmonella*

1189 strains or treated with the indicated reagent for certain time points. The samples were

1190 washed with PBS for several times, fixed in 4% paraformaldehyde, washed with PBS and

1191 incubated with blocking buffer (0.3% Triton-X) for around one hour. Then the sample were

1192 treated with the indicate antibody or reagent, and finally mounted on slides. Slides were

1193 imaged using an inverted confocal laser scanning microscope Zeiss LSM 900 and

1194 analyzed by Image J and ZEN Microscopy Software. The number of intracellular

1195 *Salmonella* per cell was quantified and analyzed with Opera Phenix Plus High Content

1196 Screening System.

1197

1198 **Flow Cytometry**

1199 BMDMs were properly differentiated using the protocol described previously. For flow

1200 cytometry, BMDMs were washed and resuspended in ice-cold FACS buffer (PBS

1201 supplemented with 0.5-1% BSA) at a concentration of 1-5 × 10⁶ cells/ml. Cells were

1202 incubated with fluorophore-conjugated primary antibodies (CD11b, CD86, and CD206)

1203 for 30 minutes at room temperature in the dark. Following antibody staining, cells were

1204 washed thoroughly and resuspended in FACS buffer. For fixation, samples were treated

1205 with 4% paraformaldehyde and washed with FACS buffer for 3 times prior to analysis.

1206 Data were acquired on a flow cytometer (Attune Nxt, Thermo) on the day of staining or

1207 after short-term storage at 4°C in fixative. M1 macrophages were identified as

1208 CD11b⁺CD86⁺, and M2 macrophages were analyzed based on CD11b⁺CD206⁺

1209 populations.

1210

1211 **pH modulation.** The pH of Dulbecco's Modified Eagle Medium (DMEM) or RPMI 1640

1212 Medium (Roswell Park Memorial Institute 1640 Medium) was adjusted using H+/OH-

1213 buffers and measured by a pH meter. To alter extracellular pH, cells were incubated with

1214 culture media that has been adjusted to the desired pH. To modulate intracellular pH,

1215 cells were incubated with culture medium adjusted to the desired pH, supplemented with

1216 30 mM NH_4Cl and 10 μM EIPA (5-(N-ethyl-N-isopropyl)-Amiloride) for 15 minutes.

1217 Following this, the intracellular pH was stabilized by re-incubating the cells in the pH-

1218 adjusted medium containing EIPA (10 μM) for the specified duration[26].

1219

1220 **LC-MS-based untargeted metabolomics.** Wild-type (WT) or *Mct4⁻/⁻* BMDMs (3X10⁶

1221 cells per sample) were treated with AZD3965 as indicated at Figure legends. Samples

1222 were extracted with methanol-acetonitrile-water at 2:2:1 (v/v/v). Extracts of these cells

1223 were dried in a vacuum concentrator at 4°C and analyzed using liquid chromatography-

1224 mass spectrometry (LC-MS). Data acquisition was conducted with a UHPLC system

1225   (Vanquish, Thermo Scientific) coupled to an Orbitrap mass spectrometer (Exploris 480,

1226   Thermo Scientific). LC separation utilized a Waters BEH amide column and a

1227   Phenomenex Kinetex C18 column. Mobile phases, linear gradient elution, and ESI source

1228   parameters followed previously published methods[62]. Metabolite annotation was

1229   performed using MetDNA (http://metdna.zhulab.cn/)[63,64].

1230

1231   **Statistics.** Data were analyzed by GraphPad Prism 9.0 software. Unless otherwise

1232   indicated, statistical significance was determined by two-sided Student's t test or ANOVA.

1233

1234 **Table S1. List of plasmids used in this study**

NO.	Plasmids	Reference
pD1	eGFP-itaconate-biosensor	this study
pD3	nanoluciferase-itaconate-biosensor	this study
pD257	lenti-CMV-IRG1-Myc	this study
pD11	lenti-CMV-IRG1-eGFP	this study
pD29	mcmv-mMCT1-3×Flag	this study
pD3101	mcmv-mMCT4-3×Flag	this study
pD31	pCDNA3.1-hMCT1-Flag	this study
pD32	pECMV-hMCT4-3xFlag	this study
pD389	pBAD24-mscarlet SCV reporter	this study
pD8	pRK5-IRG1-Flag	this study
pD387	lenti-CMV-Flag-mMCT1	this study
pD388	lenti-CMV-Flag-mMCT4	this study
pD411	lenti-CMV-eGFP-mMCT1	this study
pD412	lenti-CMV-eGFP-mMCT4	this study
pD279	pcDNA3.1-HA-mMCT1	this study
pD362	pcDNA3.1-HA-mMCT4	this study
pD184	pcmv-HA-RAB32	this study

1235

1236

1237

References

1   Kreimendahl, S. & Pernas, L. Metabolic immunity against microbes. *Trends Cell Biol*, doi:10.1016/j.tcb.2023.10.013 (2023).

2   Ryan, D. G. & O'Neill, L. A. J. Krebs Cycle Reborn in Macrophage Immunometabolism. *Annu Rev Immunol* **38**, 289-313, doi:10.1146/annurev-immunol-081619-104850 (2020).

3   O'Neill, L. A., Kishton, R. J. & Rathmell, J. A guide to immunometabolism for immunologists. *Nat Rev Immunol* **16**, 553-565, doi:10.1038/nri.2016.70 (2016).

4   Peace, C. G. & O'Neill, L. A. The role of itaconate in host defense and inflammation. *J Clin Invest* **132**, doi:10.1172/JCI148548 (2022).

5   Almeida, L., Dhillon-LaBrooy, A. & Sparwasser, T. The evolutionary tug-of-war of macrophage metabolism during bacterial infection. *Trends Endocrinol Metab*, doi:10.1016/j.tem.2023.11.002 (2023).

6   Qin, W. *et al.* Chemoproteomic Profiling of Itaconation by Bioorthogonal Probes in Inflammatory Macrophages. *J Am Chem Soc* **142**, 10894-10898, doi:10.1021/jacs.9b11962 (2020).

7   Liu, D. *et al.* Discovery of Itaconate-Mediated Lysine Acylation. *J Am Chem Soc* **145**, 12673-12681, doi:10.1021/jacs.3c02332 (2023).

8   Palsson-McDermott, E. M. & O'Neill, L. A. J. Gang of 3: How the Krebs cycle-linked metabolites itaconate, succinate, and fumarate regulate macrophages and inflammation. *Cell Metab*, doi:10.1016/j.cmet.2025.03.004 (2025).

9   Schuster, E. M. *et al.* TFEB induces mitochondrial itaconate synthesis to suppress bacterial growth in macrophages. *Nat Metab* **4**, 856-866, doi:10.1038/s42255-022-00605-w (2022).

10   Zhang, Z. X. *et al.* Itaconate is a lysosomal inducer that promotes antibacterial innate immunity. *Mol Cell* **82**, 2844-2857, doi:10.1016/j.molcel.2022.05.009 (2022).

11   Ruetz, M. *et al.* Itaconyl-CoA forms a stable biradical in methylmalonyl-CoA mutase and derails its activity and repair. *Science* **366**, 589-593, doi:10.1126/science.aay0934 (2019).

12   McFadden, B. A. & Purohit, S. Itaconate, an isocitrate lyase-directed inhibitor in Pseudomonas indigofera. *J Bacteriol* **131**, 136-144, doi:10.1128/jb.131.1.136-144.1977 (1977).

13   Chen, M. *et al.* Itaconate is an effector of a Rab GTPase cell-autonomous host defense pathway against Salmonella. *Science* **369**, 450-455, doi:10.1126/science.aaz1333 (2020).

14   Lian, H. *et al.* Parkinson's disease kinase LRRK2 coordinates a cell-intrinsic itaconate-dependent defence pathway against intracellular Salmonella. *Nat Microbiol* **8**, 1880-1895, doi:10.1038/s41564-023-01459-y (2023).

15   Michelucci, A. *et al.* Immune-responsive gene 1 protein links metabolism to immunity by catalyzing itaconic acid production. *Proc Natl Acad Sci U S A* **110**, 7820-7825, doi:10.1073/pnas.1218599110 (2013).

16   Mills, E. L. *et al.* Itaconate is an anti-inflammatory metabolite that activates Nrf2 via alkylation of KEAP1. *Nature* **556**, 113, doi:10.1038/nature25986 (2018).

17   Lampropoulou, V. *et al.* Itaconate Links Inhibition of Succinate Dehydrogenase with Macrophage Metabolic Remodeling and Regulation of Inflammation. *Cell Metab* **24**, 158-166, doi:10.1016/j.cmet.2016.06.004 (2016).

18   Swain, A. *et al.* Comparative evaluation of itaconate and its derivatives reveals divergent inflammasome and type I interferon regulation in macrophages. *Nat Metab* **2**, 594-602, doi:10.1038/s42255-020-0210-0 (2020).

19   Zhao, H. *et al.* Myeloid-derived itaconate suppresses cytotoxic CD8(+) T cells and promotes tumour growth. *Nat Metab* **4**, 1660-1673, doi:10.1038/s42255-022-00676-9 (2022).

20   Strelko, C. L. *et al.* Itaconic Acid Is a Mammalian Metabolite Induced during Macrophage Activation. *J Am Chem Soc* **133**, 16386-16389, doi:10.1021/ja2070889 (2011).

21   Ye, D., Wang, P., Chen, L. L., Guan, K. L. & Xiong, Y. Itaconate in host inflammation and defense. *Trends Endocrinol Metab*, doi:10.1016/j.tem.2024.02.004 (2024).

22   Chen, C. *et al.* ABCG2 is an itaconate exporter that limits antibacterial innate immunity by alleviating TFEB-dependent lysosomal biogenesis. *Cell Metab*, doi:10.1016/j.cmet.2023.12.015 (2024).

23   Lin, L., Yee, S. W., Kim, R. B. & Giacomini, K. M. SLC transporters as therapeutic targets: emerging opportunities. *Nat Rev Drug Discov* **14**, 543-560, doi:10.1038/nrd4626 (2015).

24   Song, W., Li, D., Tao, L., Luo, Q. & Chen, L. Solute carrier transporters: the metabolic gatekeepers of immune cells. *Acta Pharm Sin B* **10**, 61-78, doi:10.1016/j.apsb.2019.12.006 (2020).

25   Galetin, A. *et al.* Membrane transporters in drug development and as determinants of precision medicine. *Nat Rev Drug Discov* **23**, 255-280, doi:10.1038/s41573-023-00877-1 (2024).

26   Reddy, A. *et al.* pH-Gated Succinate Secretion Regulates Muscle Remodeling in Response to Exercise. *Cell* **183**, 62-75 e17, doi:10.1016/j.cell.2020.08.039 (2020).

27   Kumar, A. *et al.* NaCT/SLC13A5 facilitates citrate import and metabolism under nutrient-limited conditions. *Cell Rep* **36**, 109701, doi:10.1016/j.celrep.2021.109701 (2021).

28   Hu, K. *et al.* Suppression of the SLC7A11/glutathione axis causes synthetic lethality in KRAS-mutant lung adenocarcinoma. *J Clin Invest* **130**, 1752-1766, doi:10.1172/JCI124049 (2020).

29   Scopelliti, A. J., Font, J., Vandenberg, R. J., Boudker, O. & Ryan, R. M. Structural characterisation reveals insights into substrate recognition by the glutamine transporter ASCT2/SLC1A5. *Nature Communications* **9**, doi:ARTN 3810.1038/s41467-017-02444-w (2018).

30   Koepsell, H. Polyspecific organic cation transporters: their functions and interactions with drugs. *Trends Pharmacol Sci* **25**, 375-381, doi:10.1016/j.tips.2004.05.005 (2004).

31   Zeng, Y. R. *et al.* The immunometabolite itaconate stimulates OXGR1 to promote mucociliary clearance during the pulmonary innate immune response. *J Clin Invest* **133**, doi:10.1172/JCI160463 (2023).

32   Dou, X. *et al.* PDK4-dependent hypercatabolism and lactate production of senescent cells promotes cancer malignancy. *Nat Metab* **5**, 1887-1910, doi:10.1038/s42255-023-00912-w (2023).

33   Benjamin, D. *et al.* Syrosingopine sensitizes cancer cells to killing by metformin. *Sci Adv* **2**, e1601756, doi:10.1126/sciadv.1601756 (2016).

34   Bonglack, E. N. *et al.* Monocarboxylate transporter antagonism reveals metabolic vulnerabilities of viral-driven lymphomas. *Proc Natl Acad Sci U S A* **118**, doi:10.1073/pnas.2022495118 (2021).

35 Guan, X. & Morris, M. E. In Vitro and In Vivo Efficacy of AZD3965 and Alpha-Cyano-4-Hydroxycinnamic Acid in the Murine 4T1 Breast Tumor Model. *Aaps J* **22**, 84, doi:10.1208/s12248-020-00466-9 (2020).

36 Benyahia, Z. *et al.* In Vitro and In Vivo Characterization of MCT1 Inhibitor AZD3965 Confirms Preclinical Safety Compatible with Breast Cancer Treatment. *Cancers (Basel)* **13**, doi:10.3390/cancers13030569 (2021).

37 Kurth, I. *et al.* Therapeutic targeting of SLC6A8 creatine transporter suppresses colon cancer progression and modulates human creatine levels. *Science Advances* **7**, doi:ARTN eabi751110.1126/sciadv.abi7511 (2021).

38 Corti, A. *et al.* γ-Glutamyltransferase enzyme activity of cancer cells modulates L-γ-glutamyl-p-nitroanilide (GPNA) cytotoxicity. *Sci Rep-Uk* **9**, doi:ARTN 89110.1038/s41598-018-37385-x (2019).

39 Nolin, E. *et al.* Discovery of a ZIP7 inhibitor from a Notch pathway screen. *Nat Chem Biol* **15**, 179-188, doi:10.1038/s41589-018-0200-7 (2019).

40 Fernandez, H. R. *et al.* The mitochondrial citrate carrier, SLC25A1, drives stemness and therapy resistance in non-small cell lung cancer. *Cell Death Differ* **25**, 1239-1258, doi:10.1038/s41418-018-0101-z (2018).

41 Benjamin, D. *et al.* Dual Inhibition of the Lactate Transporters MCT1 and MCT4 Is Synthetic Lethal with Metformin due to NAD+ Depletion in Cancer Cells. *Cell Rep* **25**, 3047-3058 e3044, doi:10.1016/j.celrep.2018.11.043 (2018).

42 Cluntun, A. A. *et al.* The pyruvate-lactate axis modulates cardiac hypertrophy and heart failure. *Cell Metab* **33**, 629-648 e610, doi:10.1016/j.cmet.2020.12.003 (2021).

43 Wang, N. *et al.* Structural basis of human monocarboxylate transporter 1 inhibition by anti-cancer drug candidates. *Cell* **184**, 370-383 e313, doi:10.1016/j.cell.2020.11.043 (2021).

44 Gillis, C. C. *et al.* Dysbiosis-Associated Change in Host Metabolism Generates Lactate to Support Salmonella Growth. *Cell Host Microbe* **23**, 570, doi:10.1016/j.chom.2018.03.013 (2018).

45 Rosenberg, G. *et al.* Host succinate is an activation signal for virulence during intracellular infection. *Science* **371**, 400, doi:10.1126/science.aba8026 (2021).

46 Paulini, S. *et al.* The Biological Significance of Pyruvate Sensing and Uptake in Salmonella enterica Serovar Typhimurium. *Microorganisms* **10**, doi:10.3390/microorganisms10091751 (2022).

47 Joshi, C. S., Mora, A., Felder, P. A. & Mysorekar, I. U. NRF2 promotes urothelial cell response to bacterial infection by regulating reactive oxygen species and RAB27B expression. *Cell Rep* **37**, 109856, doi:10.1016/j.celrep.2021.109856 (2021).

48 Harvey, C. J. *et al.* Targeting Nrf2 signaling improves bacterial clearance by alveolar macrophages in patients with COPD and in a mouse model. *Sci Transl Med* **3**, 78ra32, doi:10.1126/scitranslmed.3002042 (2011).

49 Li, X. *et al.* Overexpression of monocarboxylate transporter 4 promotes the migration and invasion of non-carcinogenic L929 fibroblast cells. *Oncol Lett* **21**, 44, doi:10.3892/ol.2020.12305 (2021).

50 Sasaki, S. *et al.* Involvement of Histidine Residue His382 in pH Regulation of MCT4 Activity. *PLoS One* **10**, e0122738, doi:10.1371/journal.pone.0122738 (2014).

51 Krull, S., Hevekerl, A., Kuenz, A. & Prusse, U. Process development of itaconic acid production by a natural wild type strain of Aspergillus terreus to reach industrially

relevant final titers. *Appl Microbiol Biotechnol* **101**, 4063-4072, doi:10.1007/s00253-017-8192-x (2017).

52   Hajjar, S. & Zhou, X. pH sensing at the intersection of tissue homeostasis and inflammation. *Trends Immunol* **44**, 807-825, doi:10.1016/j.it.2023.08.008 (2023).

53   Geertsma, E. R., Nik Mahmood, N. A., Schuurman-Wolters, G. K. & Poolman, B. Membrane reconstitution of ABC transporters and assays of translocator function. *Nat Protoc* **3**, 256-266, doi:10.1038/nprot.2007.519 (2008).

54   Ellison, C. J., Kukulski, W., Boyle, K. B., Munro, S. & Randow, F. Transbilayer Movement of Sphingomyelin Precedes Catastrophic Breakage of Enterobacteria-Containing Vacuoles. *Curr Biol* **30**, 2974-2983 e2976, doi:10.1016/j.cub.2020.05.083 (2020).

55   Fowler, C. C. & Galan, J. E. Decoding a Salmonella Typhi Regulatory Network that Controls Typhoid Toxin Expression within Human Cells. *Cell Host Microbe* **23**, 65-76 e66, doi:10.1016/j.chom.2017.12.001 (2018).

56   Bui, M. *et al.* Rab32 modulates apoptosis onset and mitochondria-associated membrane (MAM) properties. *J Biol Chem* **285**, 31590-31602, doi:10.1074/jbc.M110.101584 (2010).

57   Baldassarre, M. *et al.* The Rab32/BLOC-3-dependent pathway mediates host defense against different pathogens in human macrophages. *Sci Adv* **7**, doi:10.1126/sciadv.abb1795 (2021).

58   Guan, X., Rodriguez-Cruz, V. & Morris, M. E. Cellular Uptake of MCT1 Inhibitors AR-C155858 and AZD3965 and Their Effects on MCT-Mediated Transport of L-Lactate in Murine 4T1 Breast Tumor Cancer Cells. *Aaps J* **21**, doi:ARTN 1310.1208/s12248-018-0279-5 (2019).

59   Silva, A. *et al.* In Vivo Anticancer Activity of AZD3965: A Systematic Review. *Molecules* **27**, doi:10.3390/molecules27010181 (2021).

60   Ran, F. A. *et al.* Genome engineering using the CRISPR-Cas9 system. *Nat Protoc* **8**, 2281-2308, doi:10.1038/nprot.2013.143 (2013).

61   Wang, X. *et al.* Heterologous Expression and Functional Analysis of Aedes aegypti Odorant Receptors to Human Odors in Xenopus Oocytes. *J Vis Exp*, doi:10.3791/61813 (2021).

62   Wang, R. *et al.* Global stable-isotope tracing metabolomics reveals system-wide metabolic alternations in aging Drosophila. *Nat Commun* **13**, 3518, doi:10.1038/s41467-022-31268-6 (2022).

63   Zhou, Z. W. *et al.* Metabolite annotation from knowns to unknowns through knowledge-guided multi-layer metabolic networking. *Nature Communications* **13**, doi:ARTN 665610.1038/s41467-022-34537-6 (2022).

64   Shen, X. T. *et al.* Metabolic reaction network-based recursive metabolite annotation for untargeted metabolomics. *Nature Communications* **10**, doi:ARTN 151610.1038/s41467-019-09550-x (2019).

65   Rothhammer, V. *et al.* Microglial control of astrocytes in response to microbial metabolites. *Nature* **557**, 724-728, doi:10.1038/s41586-018-0119-x (2018).